Importance of Horizontally Inhomogeneous Environmental Initial Conditions to Ensemble Storm-Scale Radar Data Assimilation and Very Short-Range Forecasts

DAVID J. STENSRUD

NOAA/National Severe Storms Laboratory, Norman, Oklahoma

JIDONG GAO

Center for Analysis and Prediction of Storms, University of Oklahoma, Norman, Oklahoma

(Manuscript received 8 April 2009, in final form 14 October 2009)

ABSTRACT

The assimilation of operational Doppler radar observations into convection-resolving numerical weather prediction models for very short-range forecasting represents a significant scientific and technological challenge. Numerical experiments over the past few years indicate that convective-scale forecasts are sensitive to the details of the data assimilation methodology, the quality of the radar data, the parameterized microphysics, and the storm environment. In this study, the importance of horizontal environmental variability to very short-range (0–1 h) convective-scale ensemble forecasts initialized using Doppler radar observations is investigated for the 4–5 May 2007 Greensburg, Kansas, tornadic thunderstorm event. Radar observations of reflectivity and radial velocity from the operational Doppler radar network at 0230 UTC 5 May 2007, during the time of the first large tornado, are assimilated into each ensemble member using a three-dimensional variational data assimilation system (3DVAR) developed at the Center for Analysis and Prediction of Storms (CAPS). Very short-range forecasts are made using the nonhydrostatic Advanced Regional Prediction System (ARPS) model from each ensemble member and the results are compared with the observations. Explicit three-dimensional environmental variability information is provided to the convective-scale ensemble using analyses from a 30-km mesoscale ensemble data assimilation system. Comparisons between convective-scale ensembles with initial conditions produced by 3DVAR using 1) background fields that are horizontally homogeneous but vertically inhomogeneous (i.e., have different vertical environmental profiles) and 2) background fields that are horizontally and vertically inhomogeneous are undertaken. Results show that the ensemble with horizontally and vertically inhomogeneous background fields provides improved predictions of thunderstorm structure, mesocyclone track, and low-level circulation track than the ensemble with horizontally homogeneous background fields. This suggests that knowledge of horizontal environmental variability is important to successful convective-scale ensemble predictions and needs to be included in real-data experiments.

1. Introduction

The development and evolution of convective storms is strongly tied to the environment in which the storms develop, as shown by numerical simulations (Weisman and Klemp 1984) and analyses of proximity soundings (Rasmussen and Blanchard 1998; Thompson et al. 2003). Environmental characteristics measured by thermodynamic instability, vertical wind shear, and mesoscale and small-scale forcing for upward motion all influence convective storm dynamics, and changes in any of these characteristics alter expectations for storm growth and development. This link between storm behavior and environmental characteristics is one reason why real-time monitoring of the environment is an important component in convective storm forecasting because the storm environment can change rapidly in both time and space (e.g., Brooks et al. 1994; Thompson and Edwards 2000; Stensrud and Weiss 2002).

Although general inferences regarding the mode of convection, storm motion, and the potential for severe weather can be made from environmental information, observed storm evolution does not always match these

Corresponding author address: Dr. David Stensrud, National Severe Storm Laboratory, National Weather Center, 120 David L. Boren Blvd., Norman, OK 73072.
E-mail: david.stensrud@noaa.gov

DOI: 10.1175/2009MWR3027.1

© 2010 American Meteorological Society

expectations (Johns and Hart 1993). This situation has led to the hope that convection-resolving numerical weather prediction (NWP) models, which explicitly predict storm growth and development given the environmental conditions, can provide improved short-range forecast guidance. This deterministic numerical prediction of convective storms, in which the actual storm structures are initialized in the model using finescale observations from Doppler radars and other sensing systems, has been explored with nonhydrostatic convection-resolving models for over a decade (e.g., Lin et al. 1993; Sun and Crook 1998; Xue et al. 2003; Alberoni et al. 2003; Dowell et al. 2004; Crook and Sun 2004; Dowell and Wicker 2009). Results from these studies indicate that the accurate 0–1-h deterministic prediction of storm evolution is challenging, owing to rapid forecast error growth in which errors can double in 10–20 min (Snyder and Zhang 2003).

The rapid error growth found in storm-scale forecasts is often attributed to errors in model physical process parameterizations, particularly those for moist precipitation (Dowell et al. 2004). However, errors in the environmental conditions also likely contribute to error growth and hamper the accurate prediction of storm characteristics. Many of the convective storm modeling studies that were mentioned previously assume horizontally homogeneous and temporally constant environmental conditions, as provided by an observed near-storm sounding. Thus, any rapid temporal and spatial changes in environmental conditions are not captured in these studies and likely influence the accuracy of the resulting forecasts. Recent results by Aksoy et al. (2009) illustrate that even simple representations of mesoscale environmental uncertainty are critical to producing accurate analyses of convective weather events from radar observations.

One forecast approach that allows for the inclusion of uncertainties in both model physical process parameterization schemes and environmental initial and boundary conditions is ensemble forecasting. Ensembles produce multiple, concurrently valid forecasts starting from slightly different initial and boundary conditions and/or somewhat different model configurations. Ensembles are one method for providing situation-dependent probabilistic forecast guidance (Brooks et al. 1995; Stensrud et al. 2000; Du and Tracton 2001; Hamill et al. 2000; Hou et al. 2001; Krishnamurti et al. 2001; Lewis 2005; Yussouf and Stensrud 2006; Stensrud and Yussouf 2007). However, the majority of ensemble applications have focused upon synoptic-scale and mesoscale weather phenomena, using model grid spacing that cannot explicitly resolve convective storms.

Storm-scale ensemble forecasting using a convection-resolving model initialized with horizontally homogeneous environments is shown to be beneficial by Elmore et al. (2002, 2003). Their results show that when storm lifetimes of at least 60 min are used as a proxy for severe weather reports, the ensemble shows considerable skill at identifying days that are likely to produce severe weather. Using the Advanced Regional Prediction System (ARPS; Xue et al. 2000, 2001, 2003), full-physics storm-scale ensembles that include terrain, horizontally varying initial conditions, and the assimilation of real observations—particularly from Weather Surveillance Radar-1988 Doppler (WSR-88D) data—have been evaluated by Kong et al. (2006, 2007). Though only five-member ensembles are employed using a scaled, lagged average forecasting technique, they find that the ensembles with a 3-km grid spacing can capture explicitly the details of storm evolution in good agreement with observations and better than any single ensemble member. Numerous studies suggest that the quality of the storm-scale analyses and forecasts are sensitive to the parameterized microphysics, the details of the assimilation methodology, the quality of radar data, the method used to generate the initial ensemble members, and the storm environment (Snyder and Zhang 2003; Dowell et al. 2004; Hu and Xue 2002; Kong et al. 2007; Aksoy et al. 2009).

In this study, we further investigate the importance of the storm environment to very short-range (0–1 h) storm-scale radar data assimilation and forecasting by including environmental variability within a three-dimensional variational data assimilation system (3DVAR) and a cloud analysis package developed at the Center for Analysis and Prediction of Storms (CAPS). The ARPS 3DVAR system (Gao et al. 2004) is used to assimilate WSR-88D data at 0230 UTC 5 May 2007 from the Greensburg, Kansas, tornadic thunderstorm into the ARPS model. Both reflectivity and radial velocity data are assimilated. An ensemble approach of increasing initial condition complexity is used to examine the importance of mesoscale environmental variability on storm-scale radar data assimilation and prediction. Ensembles of 3DVAR analyses and 1-h forecasts are produced using 1) 30 vertical environmental soundings extracted from a 30-member mesoscale ensemble Kalman filter (EnKF) data assimilation system valid at Greensburg and 2) 30 3D fields that represent the heterogeneous environment around Greensburg as extracted from the same mesoscale ensemble assimilation system. For the 30-sounding ensemble, the boundary conditions are provided from the 30 environmental soundings and do not vary with time. For the 3D ensemble, hourly boundary conditions are provided by the mesoscale ensemble data assimilation system. The very short-range (0–1 h) storm-scale ensemble forecasts are compared with 3DVAR analyses

to examine the importance of environmental variability to the accurate prediction of the tornadic supercell thunderstorm.

Section 2 provides an overview of the tornadic supercell thunderstorm event, whereas section 3 describes both the storm-scale and mesoscale data assimilation systems and experiment design. Ensemble results and qualitative performance are assessed in section 4. A final discussion is found in section 5.

2. The Greensburg tornadic supercell thunderstorm

The 4–5 May 2007 Greensburg tornadic supercell thunderstorm case is selected for study because it is well documented and produced one of the strongest tornadoes in recent years. The storm complex produced 18 tornadoes in the Dodge City forecast area, which covers most of southwestern Kansas and 47 tornado reports in Kansas, Nebraska, and Missouri (McCarthy et al. 2007). The violent tornado reported on this day started moving through Greensburg at 0245 UTC 5 May 2007 (21:45 CDT 4 May) and destroyed over 90% of the town. The tornado damage was given a rating of 5 on the Enhanced Fujita scale (EF5), which is the highest rating (McCarthy et al. 2007). Lemon and Umscheid (2008) indicate that this tornado first touched down south of Greensburg near 0200 UTC and had a total pathlength of over 53 km.

The synoptic setting for this event at 0000 UTC 5 May consisted of a deep trough over the western United States with an upper-level shortwave trough starting to move over western Kansas (Fig. 1a). A surface low was present over southeastern Colorado, and a quasi-stationary front extended from the low across northwest Kansas and into northeast Nebraska (Fig. 1b). A dryline stretched generally southward across western Kansas, Oklahoma, and into west Texas. A very moist and unstable air mass was found east of the dryline, where values of surface-based convective available potential energy (CAPE) were above 4000 J kg^{-1} across central Oklahoma and south-central Kansas. The values of 0–3-km storm-relative environmental helicity (SREH) were in excess of 150 m^2 s^{-2} throughout much of Oklahoma and Kansas, providing an environment favorable for supercell thunderstorms.

Initial storm development occurred over the northern Texas Panhandle/Oklahoma border around 2210 UTC on 4 May 2007. A complex cell evolution ensued, in which several storm splits were observed in succession over the next 2 h. As one of the storms crossed the border into Kansas near 0040 UTC, it split with the right-moving storm evolving into the tornadic supercell thunderstorm that passed over Greensburg. This storm moved from 212° at 13 m s^{-1} and developed its hook echo signature by 0106 UTC. Between 0130 and 0148 UTC, a strong midlevel mesocyclone was very clear and persistent in the data of the Dodge City WSR-88D radar (not shown). The supercell was observed to take on a classic hook echo shape by 0230 UTC as the strength of its rotation increased dramatically. The tornado that eventually produced the violent EF5 damage at Greensburg was first observed near 0200 UTC (Fig. 2; Lemon and Umscheid 2008). Forecasters at the National Weather Service Dodge City Weather Forecast Office issued a tornado warning with 30-min lead time for this event.

The storm environment at 0200 UTC 5 May near Greensburg is estimated by Lemon and Umscheid (2008). They modify the observed 0000 UTC Dodge City sounding with surface observations taken near Greensburg and obtain a CAPE estimate of over 5000 J kg^{-1}. This modified sounding also yields a 0–6-km total shear magnitude of 34 m s^{-1}, which is supportive of supercell thunderstorms. A forecast sounding from the North American Model (NAM) suggests 0–1-km SREH values had increased to over 180 m^2 s^{-2} by 0200 UTC and continued to increase, reaching values in excess of 270 m^2 s^{-2} an hour later. The large instability, strong 0–6-km wind shear and large values of 0–1-km SREH are very supportive of tornadic supercell thunderstorms (Thompson et al. 2003).

Over the next hour, from 0230 to 0330 UTC, this tornadic supercell thunderstorm (which we call the dominant storm) turned a bit more to the right, moving from 219° as the storm motion slowly decreased from 10 to near 8 m s^{-1} (Lemon and Umscheid 2008). In comparison, the group of nonsupercell thunderstorms to the northwest of the dominant storm moved much faster at 23 m s^{-1} from 206°. While the violent EF5 tornado that hit Greensburg dissipated near 0305 UTC, a second strong EF3 tornado developed near 0303 UTC, lasted for 65 min, and had a pathlength of over 43 km (Fig. 2). A third strong tornado, rated as EF3, developed at 0339 UTC in association with the same supercell and prior to the dissipation of the second tornado, and had a total path length of over 33 km. The process of producing a series of tornadoes from the same supercell thunderstorm, called cyclic tornadogenesis, has been observed both observationally (Burgess et al. 1982; Dowell and Bluestein 2002) and in numerical simulations (Adlerman et al. 1999).

The 1-h period from 0230 to 0330 UTC is selected for study since this dominant thunderstorm has classic supercell characteristics, including a well-defined mesocyclone and hook echo during this time period (Fig. 3). In addition, the storm motion is fairly steady and strong tornadoes are observed throughout the period. Thus,

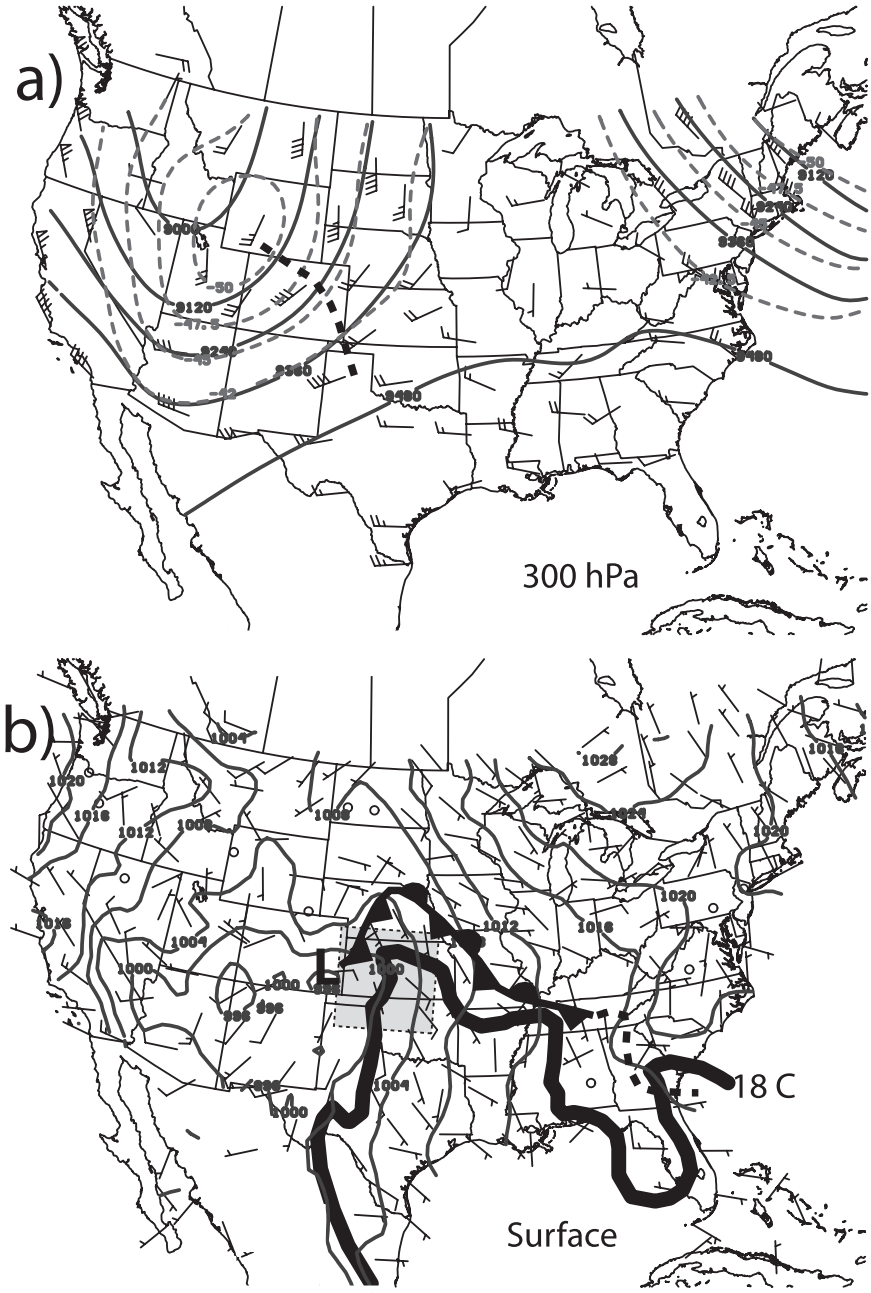

FIG. 1. Environmental conditions at 0000 UTC 5 May 2007 shown by (a) 300-hPa geopotential height (every 120 m), temperature (dashed lines every 2.5°C), and winds (full barb is 10 m s^{-1}), and (b) surface observations of MSL pressure (every 4 hPa), winds (full barb is 10 m s^{-1}), and the 18°C dewpoint isoline. Location of the largest forecast grid shown by a shaded square outlined with thin dashed lines in Oklahoma and Kansas.

this 1-h period represents a very good test for a convective-scale ensemble forecast system for a mature supercell thunderstorm event. However, the influences of the storm environment on this supercell are uncertain. One could argue that the intense, long-lived nature of this supercell indicates that it must be relatively insensitive to changes in its environment because the observed horizontal environmental variations (discussed later) do not appear to alter the characteristics of the supercell. However, it could also be that the attendant thunderstorm circulations favorably modify the near-storm environment (e.g., Brooks et al. 1994), making

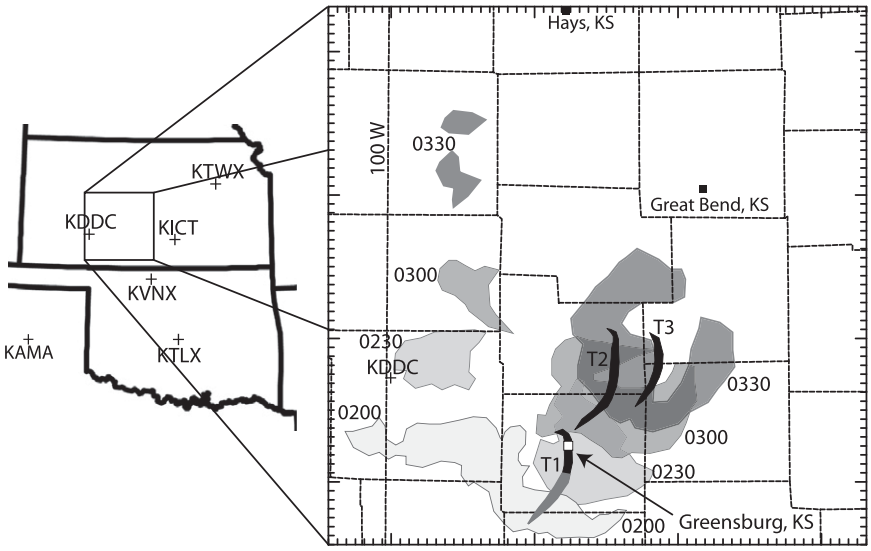

FIG. 2. Evolution of the observed tornadic supercell thunderstorm from 0200 to 0330 UTC 5 May 2007 over western Kansas with regions of composite radar reflectivity >50 dBZ shaded every 30 min. Tornado tracks as diagnosed by Lemon and Umscheid (2008) are shown (T1, T2, and T3). The T1 tornado touches down at 0200 and ends at 0305 UTC (the portion of the T1 track shaded gray occurs prior to 0230). The T2 tornado touches down at 0303 and ends at 0408 UTC, whereas the T3 tornado touches down at 0339 and ends at 0437 UTC. The locations of Greensburg, Great Bend, and Hays are noted, along with the locations of KDDC, KICT, KTWX, KVNX, KTLX, and KAMA WSR-88Ds. The enlarged domain depicts the analysis and forecast region shown in Figs. 3 and 6–15.

the environmental conditions less important once the storm reaches maturity. In this case, the modifications to the near-storm environment produced by the supercell may not be well captured by the available observational data and the data assimilation methodology, suggesting that the environment provided to the numerical model may still influence the model forecasts during this initial forecast period. In contrast, one could also argue that the supercell is sensitive to the storm environment regardless of the strength of any attendant circulations and simply responds to environmental variations in ways that are hard to observe using Doppler radar observations. In this case, numerical model simulations may provide a more reasonable assessment of storm environment sensitivity.

3. Ensemble data assimilation system and experiment design

a. Mesoscale model and ensemble data assimilation system

The modeling component of the mesoscale ensemble data assimilation system uses the nonhydrostatic Advanced Research version of the Weather Research and Forecasting (WRF-ARW) model (Klemp 2004). The WRF model includes a variety of options for physical process parameterization schemes and is recognized as the community model for mesoscale research and operational forecasting in the United States. The data assimilation component of the mesoscale ensemble data assimilation systems uses the Data Assimilation Research Testbed (DART) developed at the National Center for Atmospheric Research (NCAR). The DART uses an ensemble Kalman filter (Evensen 1997) to update the probability distribution of an atmospheric state given an observation (and its associated error) and a prior estimate of the state's probability distribution. The prior probability distribution is estimated from the statistics of an ensemble, thereby incorporating flow-dependent covariance information. Flow-dependent covariances lead to analysis increments that respect the structures of dynamically important model features. Further details on the DART ensemble Kalman filter algorithm can be found in Anderson and Collins (2007).

Hourly mesoscale ensemble analyses are produced using WRF-DART on a 30-km grid of 160 × 130 horizontal points and 30 vertical levels that cover the contiguous United States. A 30-member ensemble is used starting from initial and boundary conditions provided by NAM of the National Centers for Environmental Prediction (NCEP) at 1200 UTC 4 May 2007. Initial and boundary conditions are perturbed using the approach

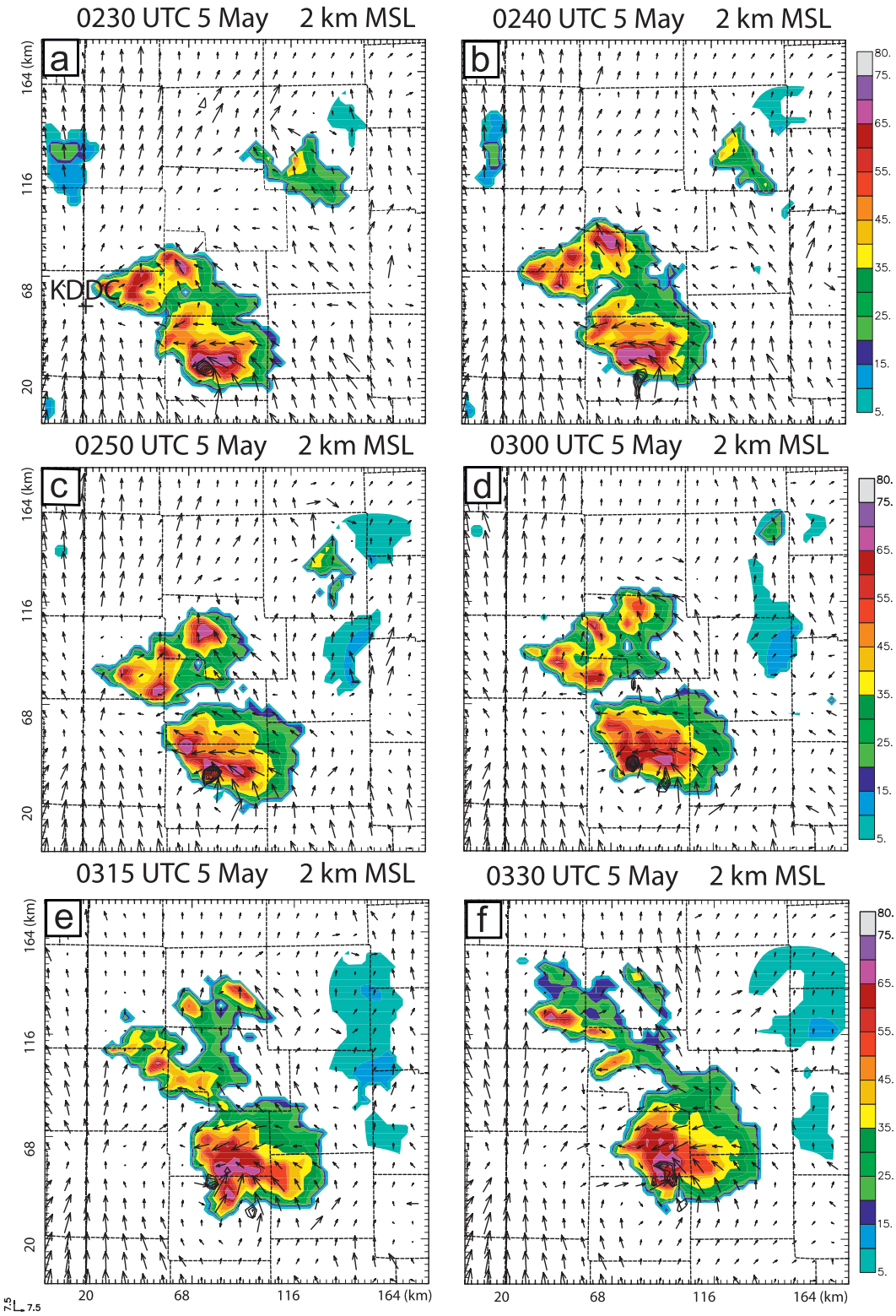

FIG. 3. Analyzed radar reflectivity (dBZ), horizontal wind vectors (m s^{-1}), and vorticity isolines (s^{-1}) at 2 km MSL using data from the KDDC, KAMA, KICT, KVNX, KTLX, and KTWX Doppler radars valid at (a) 0230, (b) 0240, (c) 0250, (d) 0300, (e) 0315, and (f) 0330 UTC 5 May 2007 over western Kansas. Analyses created using the 3DVAR system. The domain and radar locations are depicted in Fig. 2.

of Torn et al. (2006) and soil moisture is perturbed using a Monte Carlo approach following Stensrud et al. (2000). In addition to perturbing the initial and boundary conditions, the WRF-model physical process schemes also are perturbed. Variations in land surface, planetary boundary layer, radiation, convection, and microphysical parameterizations are used to create a different set of model physics for each ensemble member, as in Stensrud et al. (2000) and Fujita et al. (2007), to limit the problems caused by underdispersion seen in other ensemble systems. Details on this mesoscale ensemble system are found in Stensrud et al. (2009).

Following Fujita et al. (2007), surface observations of potential temperature, dewpoint temperature, and u and v wind components are assimilated each hour from 1300 UTC 4 May to the final analysis time of 0400 UTC 5 May. This 16-h assimilation period allows the ensemble member perturbations to evolve according to the model dynamics, while the error growth is restrained through the assimilation of surface observations. Results from Stensrud et al. (2009) indicate that this ensemble analysis approach yields realistic mesoscale structures and soundings throughout the 18-h period studied for several convective events. Thus, the hourly mesoscale ensemble analyses, valid from 0200 through 0400 UTC 5 May, should capture the observed low-level environmental variability from the surface observation assimilation, while also providing an estimate of the uncertainty of this variability.

b. *The convection-resolving model, 3DVAR, and the cloud analysis system*

The convection-resolving numerical model and data assimilation system used in this study is the three-dimensional, nonhydrostatic compressible ARPS (Xue et al. 2000, 2001) and its 3DVAR data assimilation system that includes a complex cloud analysis package (Gao et al. 2002, 2003, 2004; Brewster et al. 2005; Hu et al. 2006b). Although more advanced techniques such as four-dimensional variational data assimilation (Sun and Crook 1998) and EnKF (Synder and Zhang 2003) can also be used to assimilate radar data, a 3DVAR is selected because of its demonstrated success in radar data assimilation (Gao et al. 2004; Xiao et al. 2005; Hu et al. 2006b; Hu and Xue 2007; Montmerle and Faccani 2009; Zhao and Xue 2009) and its computational efficiency, which allows the use of relatively large model domains on available computers. Relatively large convection-resolving model domains are needed to minimize the effects of lateral boundaries on the horizontal environmental variability over the forecast time period.

The ARPS 3DVAR system, designed especially for storm-scale data assimilation, uses a recursive filter (Purser et al. 2003a,b) with a mass continuity equation and other constraints that are incorporated into a cost function, yielding three-dimensional analyses of the wind components and other model variables. Multiple analysis passes are used that have different spatial influence scales to accurately represent intermittent convective storms, although the quality control steps within the ARPS 3DVAR also are very important to improving the quality of the radial velocity and reflectivity data. By using observations from two or more National Weather Service Doppler radars scanning the same atmospheric volume simultaneously, it is possible to determine the full three-dimensional wind field from the radial velocity data alone. For all the experiments, a full volume scan of radar reflectivity and radial velocity observations completed closest to 0230 UTC from the six radars located at Dodge City, Kansas (KDDC); Vance Air Force Base, Oklahoma (KVNX); Wichita, Kansas (KICT); Oklahoma City, Oklahoma (KTLX); Amarillo, Texas (KAMA); and Topeka, Kansas (KTWX) are used in the 3DVAR. Three of these radars (KDDC, KVNX, and KICT) are within 175 km of the Greensburg supercell, thereby providing multiple simultaneous observations within the thunderstorm. Only radar data are used in the 3DVAR and the observations are used without employing intermittent assimilation cycles. Real-time convection-resolving experiments that assimilate radar observations using the ARPS 3DVAR without cycling show good results (Xue et al. 2008), suggesting that cycling may not be necessary if sufficient radar data are available. Initial testing of radar observation cycling with the Greensburg case showed mixed results (not shown), indicating that a more complete exploration of the benefits and limitations of cycling is needed in the future.

A cloud analysis package that uses radar reflectivity and other cloud observations follows the 3DVAR analysis step. The package was initially based on the local analysis and prediction system (Albers et al. 1996) and subsequently modified for the ARPS system (Zhang et al. 1998; Brewster 2002; Hu et al. 2006a). The mixing ratio of precipitation (including rainwater, snow, and hail) and potential temperature are adjusted within the cloud analysis based on reflectivity measurements. No adjustments are made to the other hydrometeor variables to avoid any negative impacts of these adjustments on the balance of model equations during the rapid analysis cycle.

Two different numerical grid domains are used to evaluate the influence of grid spacing on the predicted storm evolution using the ARPS convection-resolving model. One domain covers a 600×600 km^2 area using 3-km horizontal grid spacing (Fig. 1), whereas the other

domain covers a slightly smaller 400 × 400 km^2 area using 1-km horizontal grid spacing but centered on the same location. These two horizontal domains are large enough to contain the principal features of interest while maintaining some distance between the primary storms and the lateral boundaries. The model uses 47 terrain-following vertical layers that are stretched via a hyperbolic tangent function, yielding a vertical spacing of 100 m at the ground that expands to approximately 800 m at the top of the domain at 20 km.

c. *Experiment design*

Comparisons are made between convective-scale ensembles with the initial convective activity produced by the 3DVAR using 1) background fields that are horizontally homogeneous but vertically inhomogeneous [i.e., having different vertical environmental profiles or soundings (experiment SND)] and 2) background fields that are horizontally and vertically inhomogeneous (experiment 3D). Thus, each ensemble member is created using a different background environment but with the same radar observations being assimilated by the ARPS 3DVAR to initialize the observed convective activity. The end result is four 30-member ensembles (two at 3-km grid spacing and two at 1-km grid spacing), whose members all start with a reasonable representation of the observed convective activity, including strong updrafts and low-level rotation within the supercell thunderstorm. Forecasts created without radar data assimilation are not very valuable for the prediction of this event because none of the background fields provided by the mesoscale ensemble have an accurate depiction of the ongoing convection. Only through the use of radar data assimilation can the observed storms be created within the ensemble initial conditions.

One-hour forecasts are launched from each of the 30 ensemble members in the SND and 3D experiments (using both 3- and 1-km grid spacing) starting at 0230 UTC and ensemble results are compared with independent 3DVAR analyses. The model background fields at 0230 UTC are interpolated from the hourly mesoscale analyses valid at 0200 and 0300 UTC. The independent 3DVAR analyses of the Greensburg case are produced every 5 min from 0230 to 0330 UTC 5 May 2007 (Fig. 3) to provide an estimate of the convective circulations throughout the event. These analyses use radar observations from the 6 specified WSR-88Ds and background information from the mean of 30 3D fields provided by the mesoscale ensemble data assimilation system. No cycling is used when creating the independent analyses.

The 30 0200 UTC Greensburg soundings from WRF-DART (Fig. 4) used in experiment SND have values of CAPE between 2044 and 4832 J kg^{-1}, values of 0–3-km SREH between 216 and 525 m^2 s^{-2}, and values of 0–1-km SREH between 106 and 392 m^2 s^{-2}. Although the largest ensemble member CAPE is slightly less than the 5100 J kg^{-1} estimated from observations (Lemon and Umscheid 2008), the 0–1-km SREH value estimated from observations falls within the range of ensemble values. In addition, all the soundings are supportive of tornadic supercell thunderstorm development when evaluated using typical thermodynamic and wind shear parameters (Thompson et al. 2003), including the heights of the lifting condensation level (LCL) that vary between 183 and 1077 m.

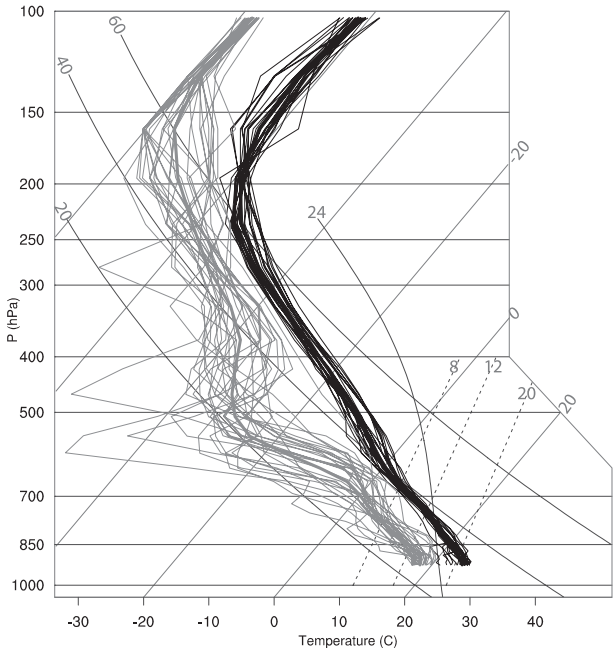

FIG. 4. Environmental soundings of temperature (black) and dewpoint temperature (gray) from 0200 UTC 5 May 2007 near Greensburg, as provided by the WRF-DART mesoscale ensemble data assimilation system. Soundings from the 30 ensemble members (thin lines) and the ensemble mean (thick lines) are shown. These soundings are used to initialize the SND ensembles.

The 30 three-dimensional environments at 0200 UTC used in experiment 3D have large horizontal variations across southwestern Kansas (Fig. 5). The axis of highest ensemble-mean CAPE stretches south–north through Greensburg, with values of 0–3-km SREH increasing both to the southwest and northeast of Greensburg (the pattern of 0–1-km SREH strongly resembles the 0–3-km SREH and is not shown). Although these gradients are not large enough to yield substantial changes in the ensemble-mean environmental parameters over the ~45-km-long path that the dominant supercell storm traversed from 0230 to 0330 UTC 5 May, the maximum change over this distance from an individual ensemble member exceeds 800 J kg^{-1} in CAPE, 300 m in LCL

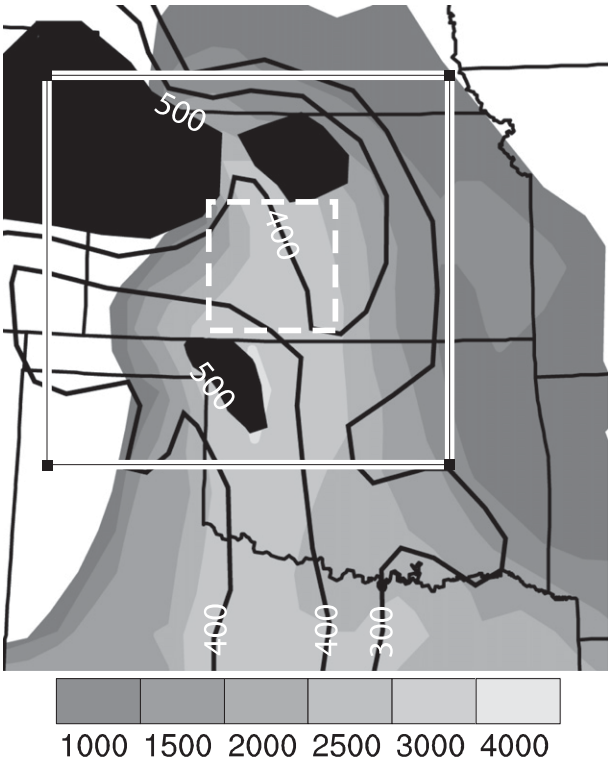

FIG. 5. Ensemble-mean analyses of CAPE (J kg^{-1}; shaded) and SREH (m^2 s^{-2}; isolines every 100 m^2 s^{-2} starting at 300 m^2 s^{-2}, and >500 m^2 s^{-2} in black fill) valid at 0200 UTC 5 May 2007. The 600 × 600 km^2 forecast domain is outlined with a white line, whereas the 180 × 180 km^2 subdomain used for subsequent model plots is outlined with a dashed white line.

height, 120 m^2 s^{-2} in 0–1-km SREH, and 150 m^2 s^{-2} in 0–3-km SREH. These gradients are large enough that changes in storm behavior may occur. Changes in other environmental variables such as temperature, relative humidity, and winds are also apparent.

4. Results

a. Experiment SND

Forecasts with 3-km grid spacing from the 30 ensemble members initialized with homogeneous environments indicate that the ensemble members tend to move the dominant storm too quickly and the storms grow upscale into a single large storm complex by the end of the 1-h forecast period (Fig. 6). Although some of the individual ensemble members have more complex structures (not shown) and suggest several cells at the end of the forecast period, there is a strong tendency among all the members to create a single large storm complex located north of the observed (dominant) supercell thunderstorm. A typical forecast from one ensemble member is used to illustrate the general behavior seen in the runs.

Within the first 10 min of the forecast, the smaller cells (located to the northwest of the southern, dominant storm) begin to merge into a larger single-cell structure (Fig. 6b). The dominant storm has a hint of a hook echo at this time; however, it loses the hooklike appendage within the next 10 min and fails to establish this structure throughout the remainder of the forecast period. Indeed, the maximum mesocyclone vorticity at 2 km mean sea level (MSL) decreases by 25% during the first 5 min of the forecast period and then remains below the initial vorticity value. Similarly, the maximum mesocyclone vorticity at 4 km MSL decreases by 40% in the first 5 min. This weakening of the midlevel mesocyclone occurs even as the updraft speeds are increasing throughout the first 15-min period. In addition, the easterly flow within the forward flank of the supercell storm at 2 km MSL, seen in the analyses at 0250 UTC (Fig. 3c), is much weaker in the predicted storm (Fig. 6c) and is absent from the predicted storm 10 min later (Fig. 6d). A southwesterly flow is found in the southwest sector of the dominant storm at 0300 UTC (Fig. 6d) in a region of downdraft behind the leading edge of the eastward-moving cold pool. This flow pattern is quite different from the northerly flow seen in the rear flank of the supercell from the analyses (Fig. 3d).

Compared to the 3DVAR analyses (Fig. 3), the dominant predicted storm moves too fast and has a more northerly motion component than observed. By 0300 UTC, the circulation center of the predicted dominant storm is nearly 15 km too far to the northeast as compared with the analyses (cf. Figs. 3d and 6d), implying an 8 m s^{-1} error in predicted storm motion. This storm motion error suggests that the predicted storm fails to develop the correct pressure-driven vertical accelerations associated with the interactions between the environmental wind shear and the updraft that lead to the deviating storm motion (Rotunno and Klemp 1982, 1985).

Part of the inability of the forecast dominant storm to maintain a strong midlevel mesocyclone likely is due to the lack of surface outflows in the model initial conditions. Because the 3DVAR analyses primarily use radar observations to initialize the in-storm structures, features near the ground surface below the radar beam are not captured unless the radar is very close to the storm. While the low-level temperature, relative humidity, and wind fields begin to be influenced by the evaporational cooling of precipitation particles to form an outflow within the first 5 min of the model forecasts, it takes time for the environment to respond to this forcing. Low-level inflow toward the storm develops outward from the thunderstorm and intensifies throughout the first 20 min.

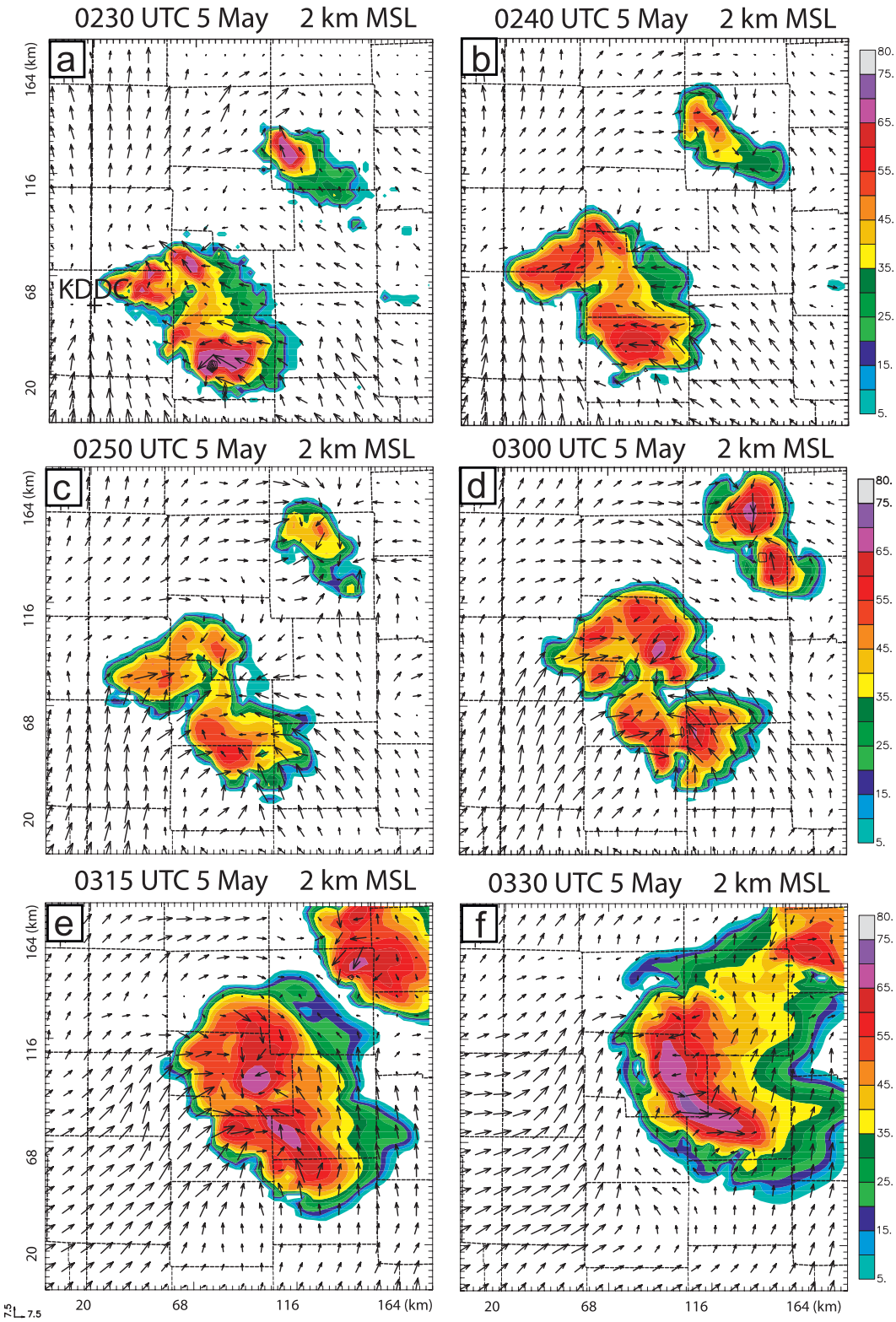

FIG. 6. As in Fig. 3, but for the SND ensemble member 3 forecast starting from the 3DVAR analysis at 0230 UTC 5 May 2007. Domain location shown in Fig. 2.

The incorrect predicted storm motion may influence the upscale growth of the storm complex between 0300 and 0330 UTC (Figs. 6d–f). Because the dominant storm fails to move to the right of the other storms, the distance separating the storms remains constant over time instead of increasing as observed (Figs. 3d–f). The closer separation of the predicted storms leads to stronger interactions between their surface outflows, such that by 0250 UTC the surface outflows are beginning to collide (not shown) and produce a linear updraft zone on the eastern edge of the surface outflows by 0300 UTC (Fig. 7). Over the next 40 min, the zone of rising motion along the eastern edge of the surface outflow assists in the upscale growth of the convective region and produces a forecast storm evolution that is very different from the observations.

The evolution of the ensemble-mean reflectivity field is very similar to that of member 3, except the reflectivity fields are generally much weaker and smoother (not shown). To measure the forecast variability, the ensemble spread of composite reflectivity is examined (Fig. 8). The ensemble spread and its evolution reflect model forecast error and its growth. Small values of spread indicate relative forecast certainty and large values of spread indicate relative forecast uncertainty. There is no spread in the 0230 UTC initial conditions (Fig. 8a) as a result of the reflectivity fields from 3DVAR being identical in all the ensemble members and the lack of any convective activity in the horizontally homogeneous background fields. However, the spread increases in both areal coverage and amplitude as the forecast time increases (Figs. 8b–f). Larger values of spread are seen circling the edges of the ensemble-mean thunderstorm positions, with the largest values of spread found in regions where storms are interacting (Fig. 8d) or on the southwestern edge of the developing storm complex (Figs. 8e,f). A comparison of Figs. 6 and 8 indicates that the smaller, interior values of spread (nearly encircled by the larger spread values) are closely aligned with the ensemble-mean location of the dominant storm. Thus, the dominant storm evolves similarly in the ensemble members with slight differences in storm speed and direction of movement. The error growth is largely located over the regions of convective boundaries, especially near the southern edge of the storms.

Because the model grid spacing of 3 km may negatively influence the ability of the predicted dominant storm to maintain a strong mesocyclone, ensemble forecasts at 1-km grid spacing are also produced and evaluated. Results from the ensemble indicate that the 1-km forecasts out to 30 min compare more favorably with the observations than the 3-km forecasts, yet the predicted storms still develop upscale into a large storm complex by the end of the 1-h forecast period (Fig. 9). The same ensemble member is again selected to characterize the typical forecast evolution. The ensemble spread field resembles that found using 3 km and so is not discussed.

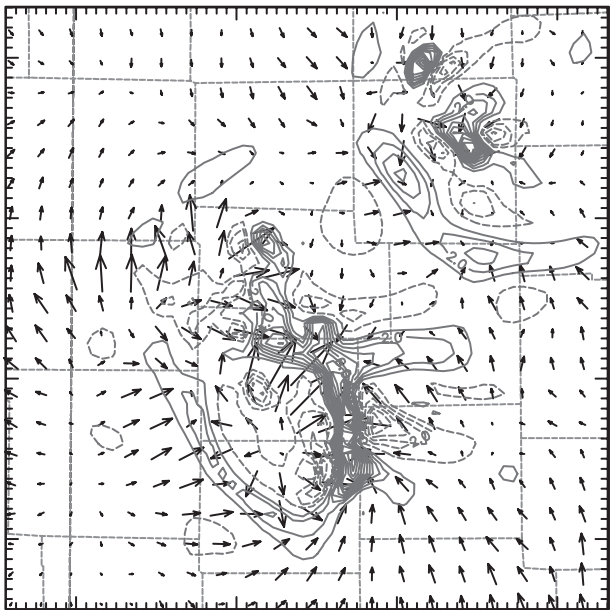

FIG. 7. Isolines of vertical motion (every 1 m s^{-1} with negative values dashed) at 2 km MSL and surface horizontal wind vectors (m s^{-1}) at 0300 UTC 5 May 2007 from SND ensemble member 3. Domain location shown in Fig. 2.

During the first 20 min of the forecast period, the storms located to the northwest of the dominant cell maintain more of their individual character (Figs. 9a–c). In addition, the forward flank of the dominant cell at 0250 UTC has a stronger easterly flow (Fig. 9c) compared to the prediction from the 3-km model (Fig. 6c). The southwesterly flow seen in the western sector of the dominant storm at 0300 UTC for 3-km grid spacing (Fig. 6d) is absent from the 1-km grid spacing prediction (Fig. 9d). However, the storms begin to grow upscale at this time and form a single large convective storm complex by 0330 UTC (Figs. 9d–f). Thus, the smaller 1-km grid spacing improves the first 30 min of the forecast; however it is unable to avert the problems that develop later in the model ensemble forecasts of this event, as the predicted surface outflows begin to dominate storm development.

The ensemble forecasts at both 3- and 1-km grid spacing can be used to determine the likelihood of low-level storm rotation throughout the 1-h forecast period, which can also help validate the conclusions drawn thus far from the prediction of a single ensemble member. Using forecast data every 5 min, the number of times any ensemble member vorticity value exceeds 0.004 s^{-1}

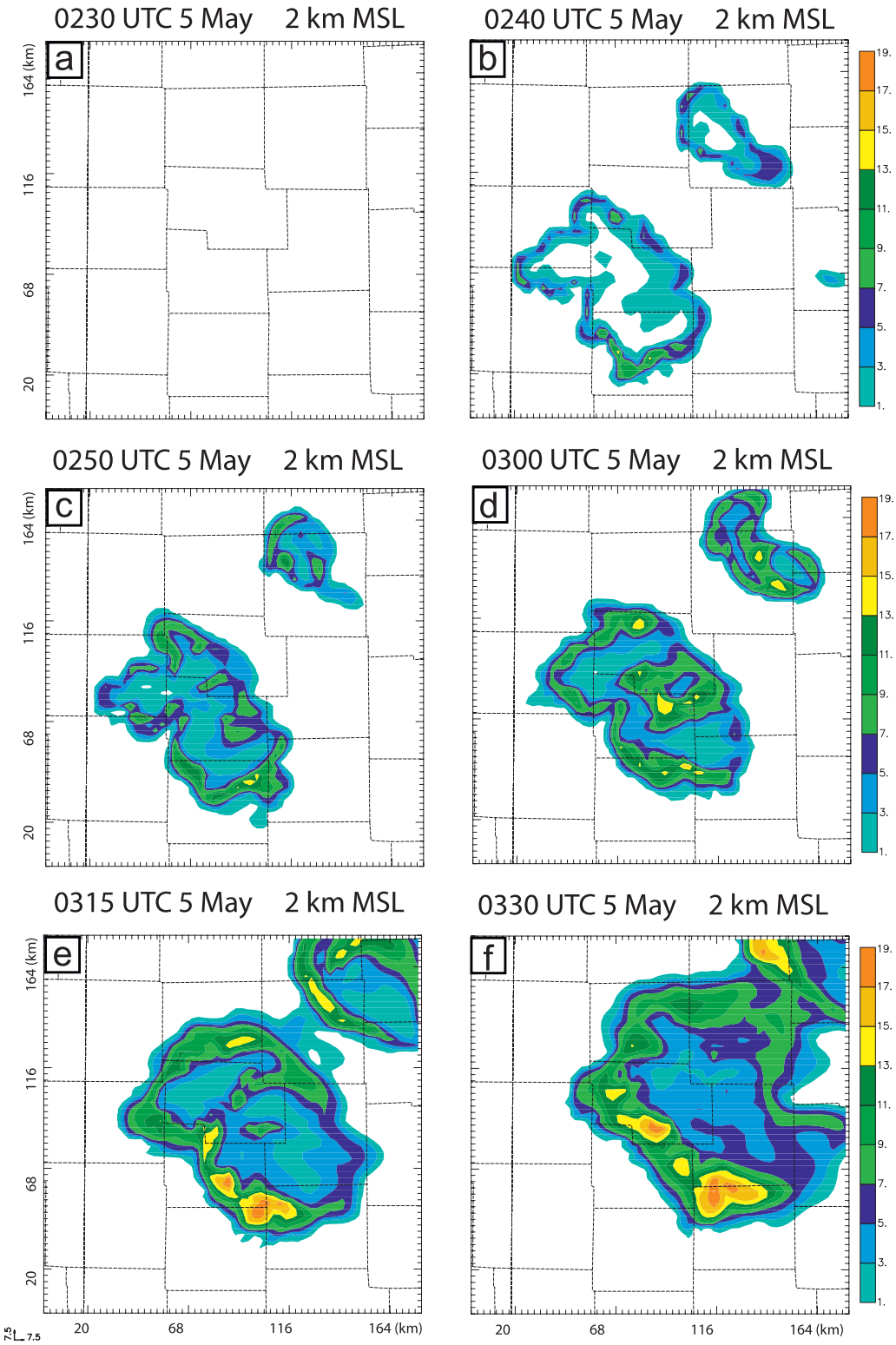

FIG. 8. The ensemble spread of reflectivity (dBZ) for the experiment SND with 3-km resolution valid at (a) 0230, (b) 0240, (c) 0250, (d) 0300, (e) 0315, and (f) 0330 UTC 5 May 2007 over western Kansas. Domain location shown in Fig. 2.

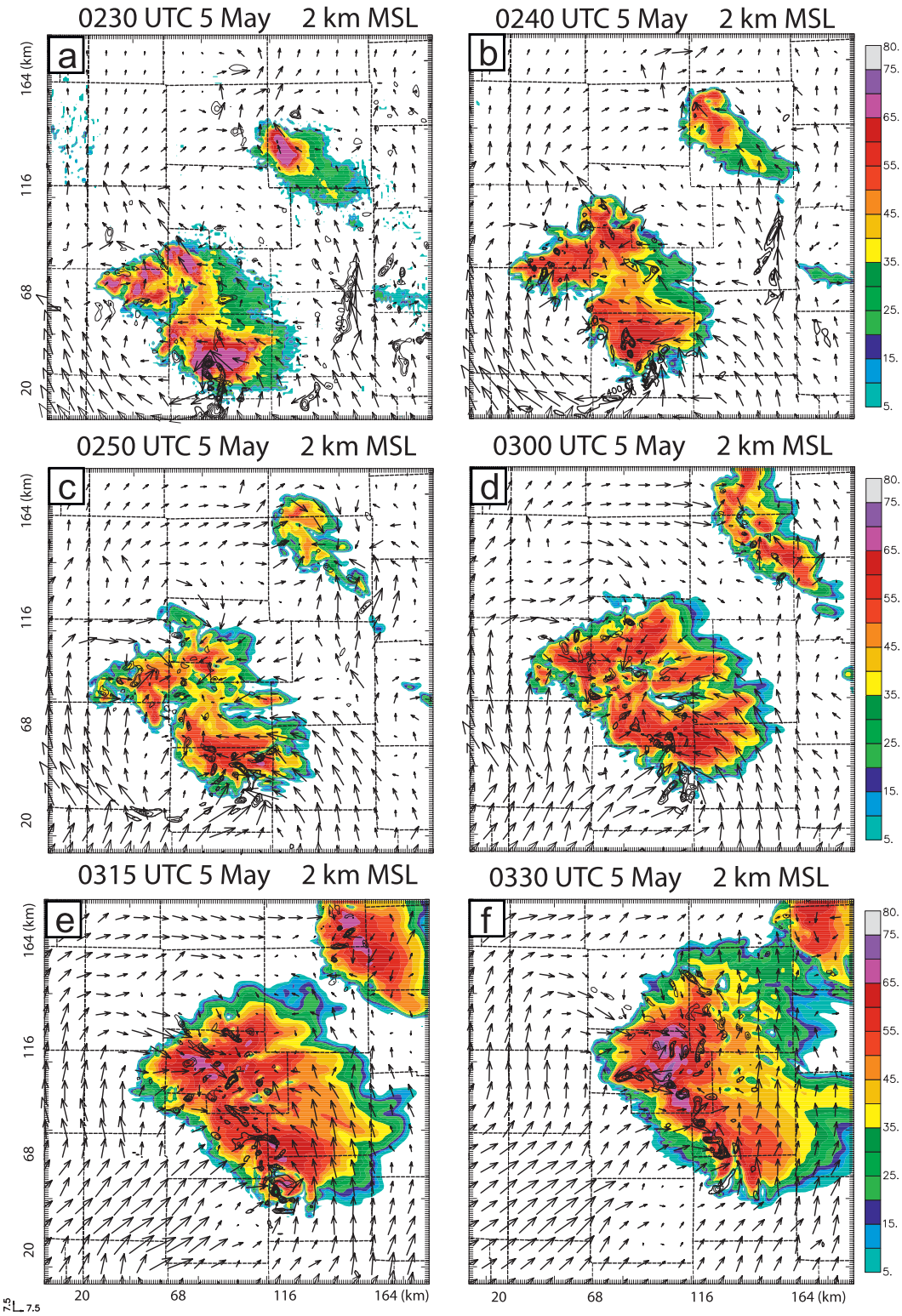

FIG. 9. As in Fig. 6, but for the 1-km grid spacing SND ensemble member 3 forecast.

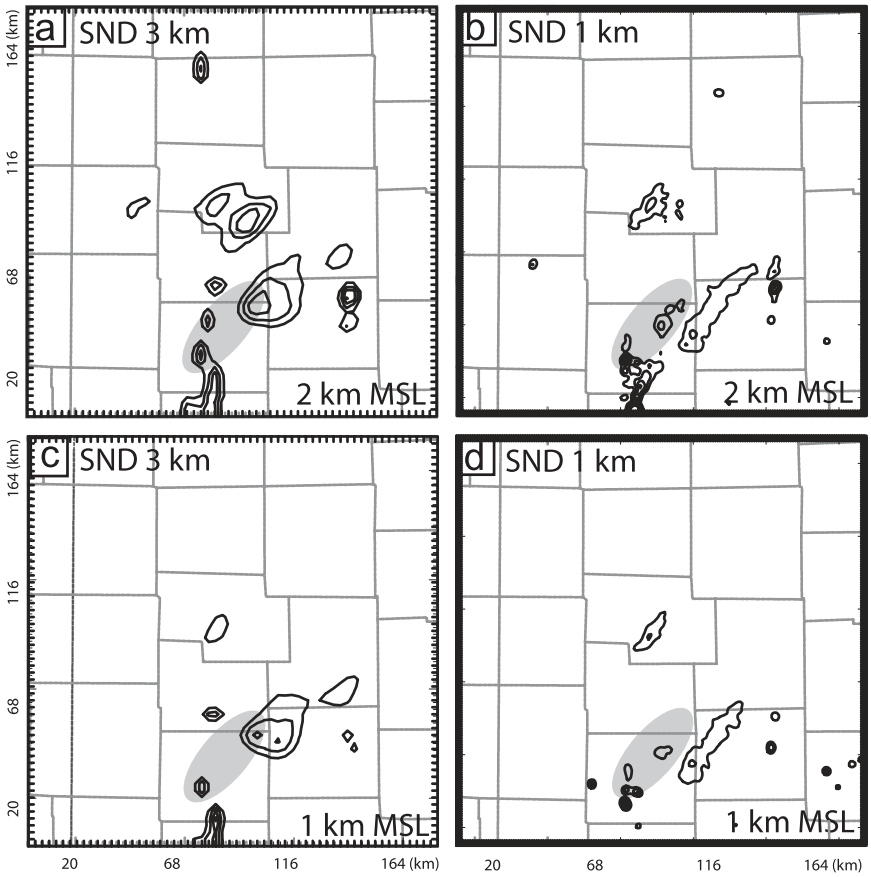

FIG. 10. Vorticity counts (isolines every 5, starting at 5) from SND ensemble for (a),(c) 3-km grid spacing and (b),(d) 1-km grid spacing between 0230 and 0330 UTC 5 May 2007. Counts valid at (top) 2 km MSL and (bottom) 1 km MSL (300–400 m above ground level). Vorticity is counted when it exceeds 0.004 s^{-1} for 3-km runs and 0.01 s^{-1} for 1-km runs at each grid point. Shading denotes approximate region of observed mesocyclone track at 2 km MSL from 3DVAR analyses. Domain location shown in Fig. 2.

for 3-km grid spacing (0.01 s^{-1} for 1-km grid spacing) are counted at each grid point for a given height level. The resulting field is noisy, so a simple five-point horizontal smoother is applied in two successive passes through the data. Results at 2 km MSL fail to show a coherent path of vorticity counts in the region of the observed mesocyclone, as would be expected for a persistent supercell thunderstorm (Figs. 10a,b). Instead, there are gaps in the count data that are consistent with the weakening of the mesocyclone soon after the forecast begins. The improved 30-min forecasts from the 1-km ensemble (Fig. 10b) are seen in the more coherent zone of vorticity counts that stretches from southwest to northeast; even though the count numbers are not large, gaps are still present, and the most coherent path is to the east of the observed mesocyclone path. For the 1 km MSL vorticity data (Figs. 10c,d), the counts can be used as a proxy for a likely tornado track as this height is only 300–400 m above ground level in western Kansas and below the mean environmental LCL height. Comparison of the 1 km MSL vorticity count track with the observed tornado tracks (Fig. 2d) again indicate that the predicted storm moves too quickly as the forecast track is approximately 14 km east of the observed tracks and is shifted northward. It is encouraging, however, that some of the ensemble members are producing strong low-level rotation not far above the ground surface.

b. *Experiment 3D*

Forecasts with 3-km grid spacing from the 30 ensemble members initialized with both horizontally and vertically inhomogeneous initial environmental conditions indicate that the ensemble member forecasts of the dominant storm are improved compared to the SND forecasts; however, the storms still grow upscale to form a single large storm complex by the end of the 1-h

forecast period (Fig. 11). A typical forecast from one ensemble member is used to illustrate the general behavior seen in the 3D runs.

As with the SND runs, the smaller cells (located to the northwest of the dominant storm) begin to merge into a larger single cell structure within 10 min (Fig. 11b). However, the midlevel mesocyclone associated with the southern dominant storm is maintained much better in the 3D runs than in the SND runs (cf. Figs. 11 and 6). In particular, the dominant storm maintains a hooklike appendage in the reflectivity field throughout most of the 1-h forecast period (Fig. 11). The maximum mesocyclone vorticity at 2 km MSL decreases by only 2% during the first 5 min of the forecast, compared to a 25% decrease in the SND run. The maximum midlevel vorticity at 6 km MSL decreases by 16% in the first 5 min and remains constant or intensifies thereafter. In addition, the observed easterly flow at 2 km MSL within the forward flank of the dominant storm is maintained out to 0250 UTC and is replaced with southeasterly flow afterward (Figs. 11c,d). No large regions of southwesterly flow are seen in the western, rear flank sector of the dominant storm. Thus, the dominant storm in the 3D run is more consistent with the observations than the dominant storm in the SND run.

Although difficult to discern on the figures, the storm motion of the dominant storm is $\sim$3 m s^{-1} slower in the 3D ensemble than in the SND ensemble and agrees better with the observations. Therefore, while both the 3D and SND runs predict a storm motion for the dominant storm that is too fast, the storm motion error is smaller in the 3D runs.

The 3D ensemble runs also are not initialized with surface outflows, and so outflows develop as evaporational cooling of precipitation particles occurs in the forecasts. In this horizontally varying environment, the surface temperatures in the outflow region are warmer than found in the SND run by several degrees Celsius. Although the surface outflows from the storms eventually converge and form a single cold pool by 0300 UTC (Fig. 12), the winds within the outflow region are weaker and the 2 km MSL vertical motion field is more representative of isolated cells than the forecast from the SND run (Fig. 7). However, the outflow eventually dominates the evolution of the storms in these forecasts, leading to the upscale growth of the convection. Yet the reduced outflow strength appears to help the dominant storm maintain a stronger low-level mesocyclone throughout the entire forecast period.

The ensemble spread of composite reflectivity for experiment 3D with 3-km resolution (Fig. 13) is greater than 1 dBZ over a larger area but has smaller maximum values after 0250 UTC, than the SND ensemble (Fig. 8). The nonzero spread values at the initial time of 0230 UTC are a result of convective activity present in the three-dimensional background fields provided by the mesoscale ensemble. In particular, eight of the ensemble members have convective activity in the northwestern portion of the domain at the initial time (not shown). This convection intensifies and moves northeastward with the environmental flow as the forecast evolves, which is reflected in the ensemble spread fields. Convective activity is also present in some ensemble members along and near the dryline that stretches northward from the southern edge of the domain. However, similar to experiment SND, larger values of spread also encircle the dominant storm that is inserted into the ensemble runs by the 3DVAR scheme. Interestingly, the maximum value of the spread encircling the dominant storm is less than that found in the SND ensemble (cf. Figs. 8e–f and 13e–f), suggesting that the evolution of the dominant storm in the 3D ensemble is more consistent than the dominant storm in the SND ensemble (as is also seen later in the vorticity count plots).

The placement of convective activity in the model background fields to the northwest of the dominant storm within several ensemble members is fortuitous, because these storms do not interact with the dominant storm and influence its behavior. If these convective regions had occurred adjacent to or on top of the dominant storm location, then convective interactions likely would have occurred and the forecast results from the 3D runs would be degraded for these members. The realization of the important role played by convective activity that exists in the background fields emphasizes the need to also use radar observations to suppress convection where it does not exist (Tong and Xue 2005; Aksoy et al. 2009).

The ensemble spread results illustrate the important role played by the background fields provided by the mesoscale ensemble. Although the evolution of the dominant storm is more consistent in the 3D ensemble than in the SND ensemble, the 3D information also produces convection in regions where it was not observed. This situation argues for the use of radar observations within the mesoscale ensemble to constrain convective activity only to areas where it is observed, as done by Fujita et al. (2008), or the use of a single high-resolution ensemble system that assimilates both mesoscale and convective-scale observations.

Results from the 1-km 3D ensemble runs (Fig. 14) are similar to the 3-km ensemble runs (Fig. 11). The storms to the northwest of the dominant storm retain more of an isolated structure in the 1-km run than seen in the 3-km run over the first 30 min of the forecast (cf. Figs. 14 and 11). The hook-like appendage is very apparent in

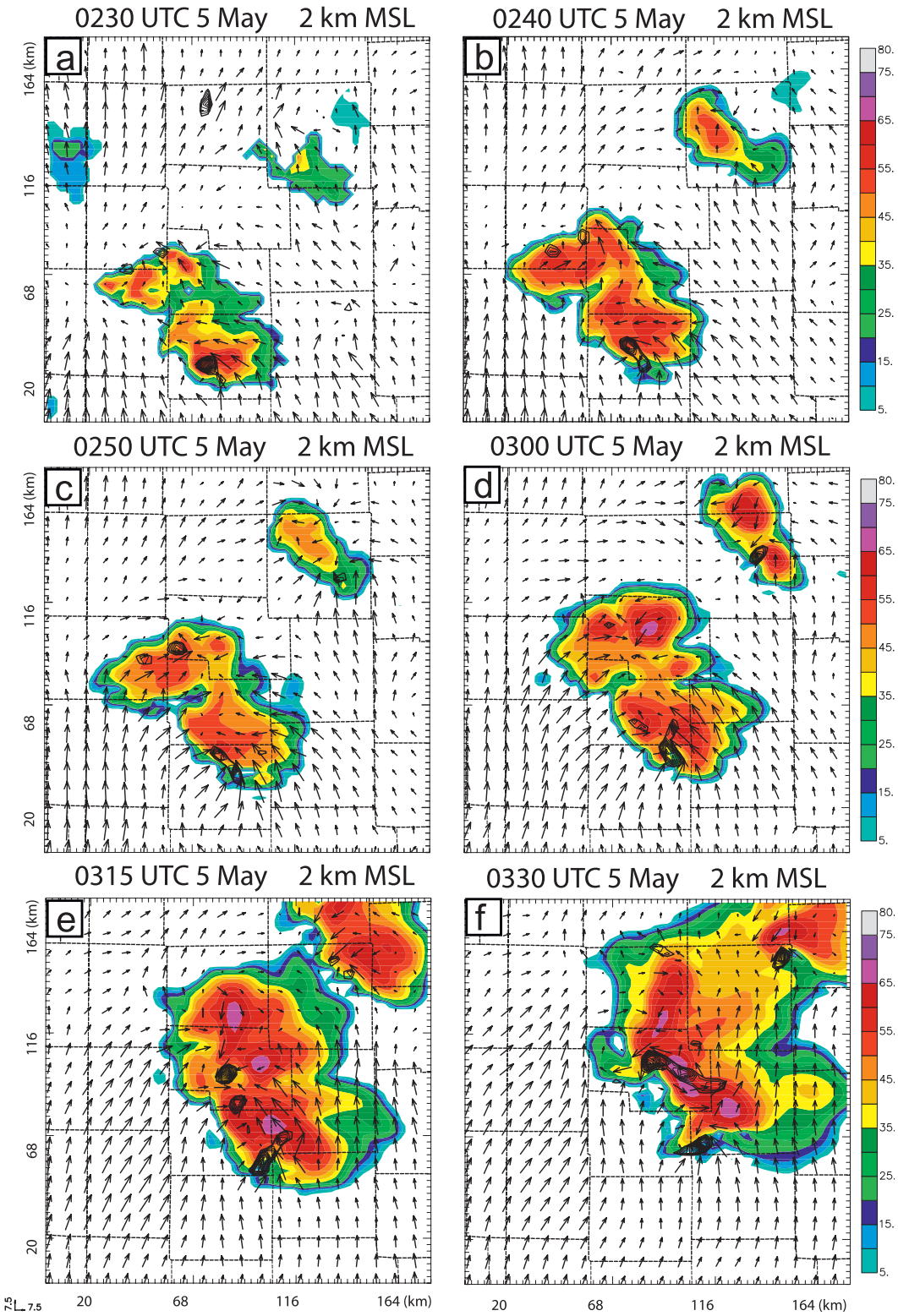

FIG. 11. As in Fig. 6, but for 3D ensemble member 3 forecast starting from the 3DVAR analysis at 0230 UTC 5 May 2007.

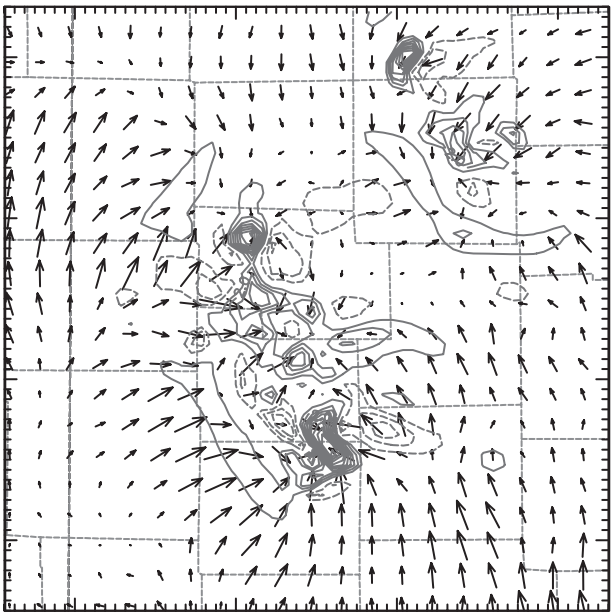

FIG. 12. As in Fig. 7, but from 3D ensemble member 3 showing isolines of vertical motion (every 1 m s^{-1} with negative values dashed) at 2 km MSL and surface horizontal wind vectors (m s^{-1}) at 0300 UTC 5 May 2007.

the 1-km runs and is depicted at every 5 min of forecast time. However, the storms still grow upscale to form a single storm complex by the end of the 1-h forecast. Yet the southern edge of this system still has a hook echo and mesocyclone at this time.

Vorticity counts from both the 3- and 1-km forecast ensembles show that the mesocyclone tracks from the 3D ensemble agree remarkably well with the observed mesocyclone track (Figs. 15a,b). Not only is the mesocyclone path more accurate but the counts are higher from the 3D runs compared to the SND runs (cf. Figs. 15 and 10), indicating that more ensemble members are producing a mesocyclone along the correct path. The 1-km 3D ensemble vorticity counts are even larger than the 3-km 3D ensemble vorticity counts, illustrating another clear advantage for the smaller grid spacing. If we use the 1 km MSL vorticity count plots as a proxy for the tornado path, then the 1-km 3D ensemble results highlight the potential for several tornadoes during this 1-h period (Fig. 15d). Although the specific paths are not in agreement with the observations (Fig. 2), the correct counties are identified and the idea that several tornadoes may develop (especially as the storm moves northward) is seen in the ensemble runs.

Assuming a storm motion of 18 m s^{-1} and a mesocyclone width of 5 km, the largest vorticity count one could expect at any grid point is 30, as the storm moves across the domain with forecast output available every 5 min (1 count per ensemble member). If the mesocyclone width is much larger than 5 km, the storm motion slower than 18 m s^{-1}, or forecast output data available more frequently, then larger counts are possible. Results from the 3D ensemble at 1-km grid spacing indicate that the maximum 1 km MSL (~300 m above ground level) vorticity count found at any grid point is 27. However, a total of only 20 grid points have count values above 15, and only 9 grid points have count values above 20. Thus, the ensemble probabilities of strong low-level rotation (>0.01 s^{-1}) are typically in the 10%–30% range, highlighting the value of an ensemble approach because a single deterministic forecast could easily miss this low-probability event.

To quantify forecast accuracy from the four ensemble forecasts, equitable threat scores (ETSs; Wilks 2006) are calculated by comparing the forecast ensembles and their means with the 3DVAR analyses for reflectivity values exceeding a 30-dBZ threshold. A perfect forecast yields an ETS value of 1, with forecast accuracy decreasing as the ETS value decreases toward 0. Results generally indicate that the 3D ensemble members and their mean have higher ETS values during the 1-h forecast period in comparison with the SND ensemble members and their mean for both 3- and 1-km grid spacing (Fig. 16). One 3D ensemble member, in particular, has much higher values of ETS than the other members after 20 min (Figs. 16b,d). However, the ETS scores for the 3D ensemble members have greater variability during the first 30 min than those for the SND ensemble members. The low ETS values for several of the 3D ensemble members are a result of convection present in the mesoscale ensemble analyses that are used to initialize the convective-scale ensemble. The quicker decrease of ETS values for the 1-km resolution than that for the 3-km resolution indicates both the more rapid divergence of the forecast storm behavior for 1-km and the expected decrease in ETS values as model grid spacing decreases (Gallus 2002).

5. Discussion

Storm-scale ensemble forecasts of a tornadic supercell thunderstorm that passed over Greensburg, Kansas, between 0230 and 0330 UTC 5 May 2007 are compared with high-resolution 3DVAR analyses to evaluate the importance of the storm environment to the resulting forecasts. Radar observations from 6 WSR-88Ds are used in a 3DVAR approach to initialize the storms at 0230 UTC 5 May, and 1-h forecasts produced for 30 ensemble members that differ only in the definitions of their initial environments. The influence of grid spacing is also examined by comparing ensembles run at 3- and 1-km grid spacing. It is found that the ensembles

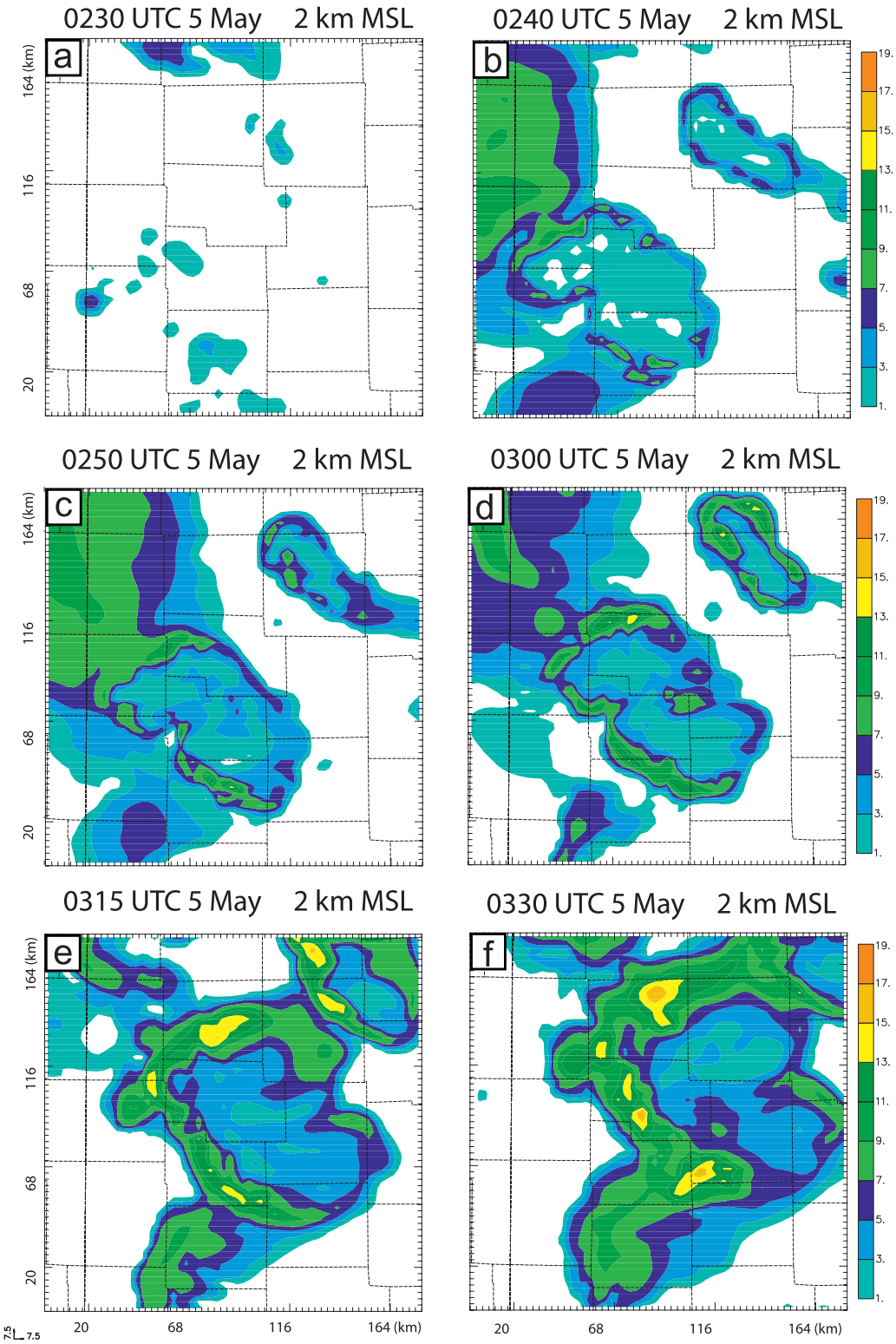

FIG. 13. As in Fig. 8, but for experiment 3D.

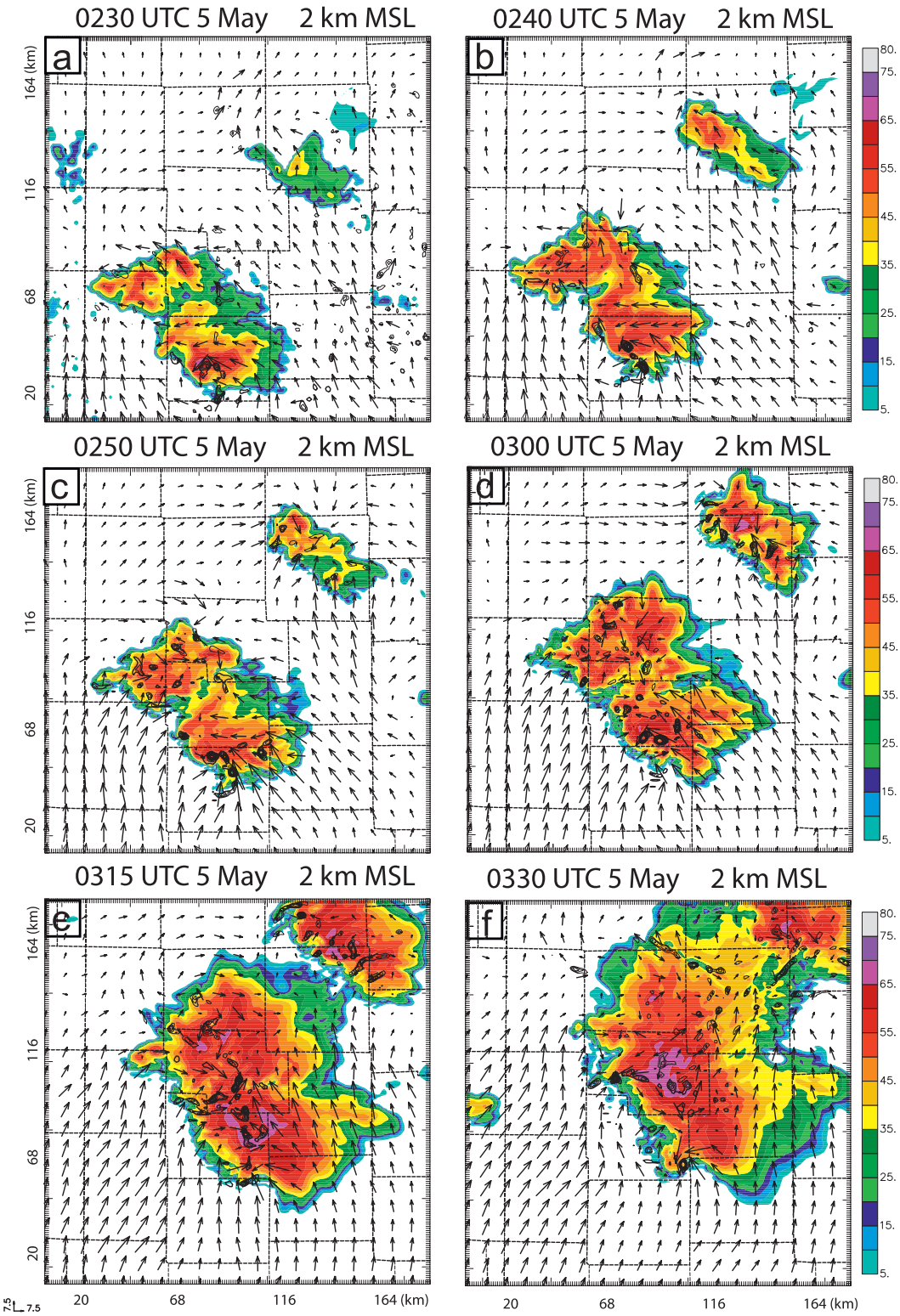

FIG. 14. As in Fig. 9, but for the 1-km grid spacing 3D ensemble member 3 forecast.

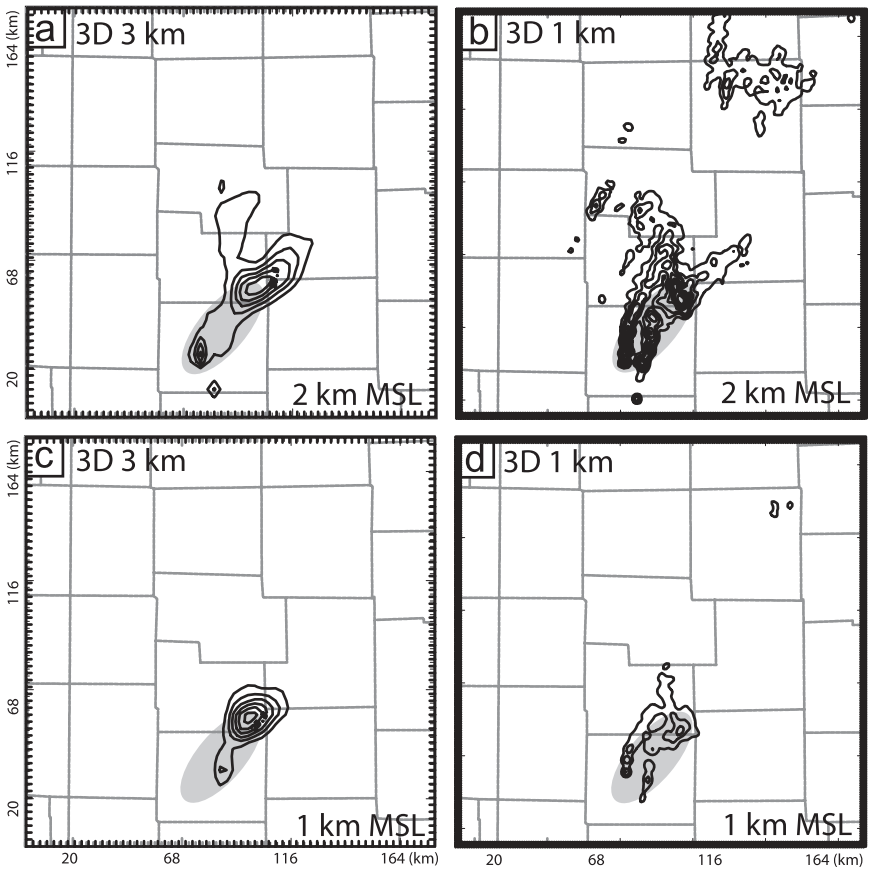

FIG. 15. As in Fig. 10, but for the 3D ensemble.

initialized with realistic three-dimensional environments compare better with observations than ensemble forecasts initialized with vertical soundings representative of the environmental conditions near the storm. Improvements are found in storm structure and evolution, mesocyclone path, equitable threat scores for reflectivity, and very low-level (~300 m) rotation tracks when three-dimensional environments are used in the ensembles. Some improvements in storm evolution and mesocyclone path are also found as the grid spacing decreases from 3 to 1 km, but the largest improvements in the ensemble forecasts are because of the inclusion of horizontal environmental variability in the environmental conditions.

Because previous studies that assimilate radar observations into convection-resolving models to make short-range forecasts typically have used horizontally homogeneous environments, these results highlight the importance of mesoscale horizontal variability to the quality of the resulting forecasts and merit serious consideration. Results show that what appear to be relatively small horizontal changes in environmental parameters play important roles in determining the strength of the surface outflow, maintaining the mid- and low-level mesocyclones and influencing storm evolution. Although the processes and feedbacks that produce these effects on storm evolution are not clear, the improvements in the forecasts are dramatic for this tornadic supercell thunderstorm event.

Results further show the value of using convective-scale ensembles for very short-range numerical weather prediction. Although the 3D ensemble forecasts nearly all produce a supercell thunderstorm, the storm track and the intensity of various important storm features (cold pools, mesocyclones, and updraft speed) are different in the various ensemble members. In particular, the probabilities of a strong, very low-level rotation calculated from the ensemble forecasts (and that could be used to identify regions of tornadogenesis) are often in the 10%–30% range. Thus, the use of a single deterministic forecast to capture such a low-probability event is likely to lead to failure. Severe weather events are inherently unlikely, and the forecast approach used must account for their unlikely nature. This conclusion is supported by other studies that note the value of an ensemble strategy for intense local weather (e.g., Brooks et al. 1995; Elmore et al. 2002, 2003; Kong et al. 2007).

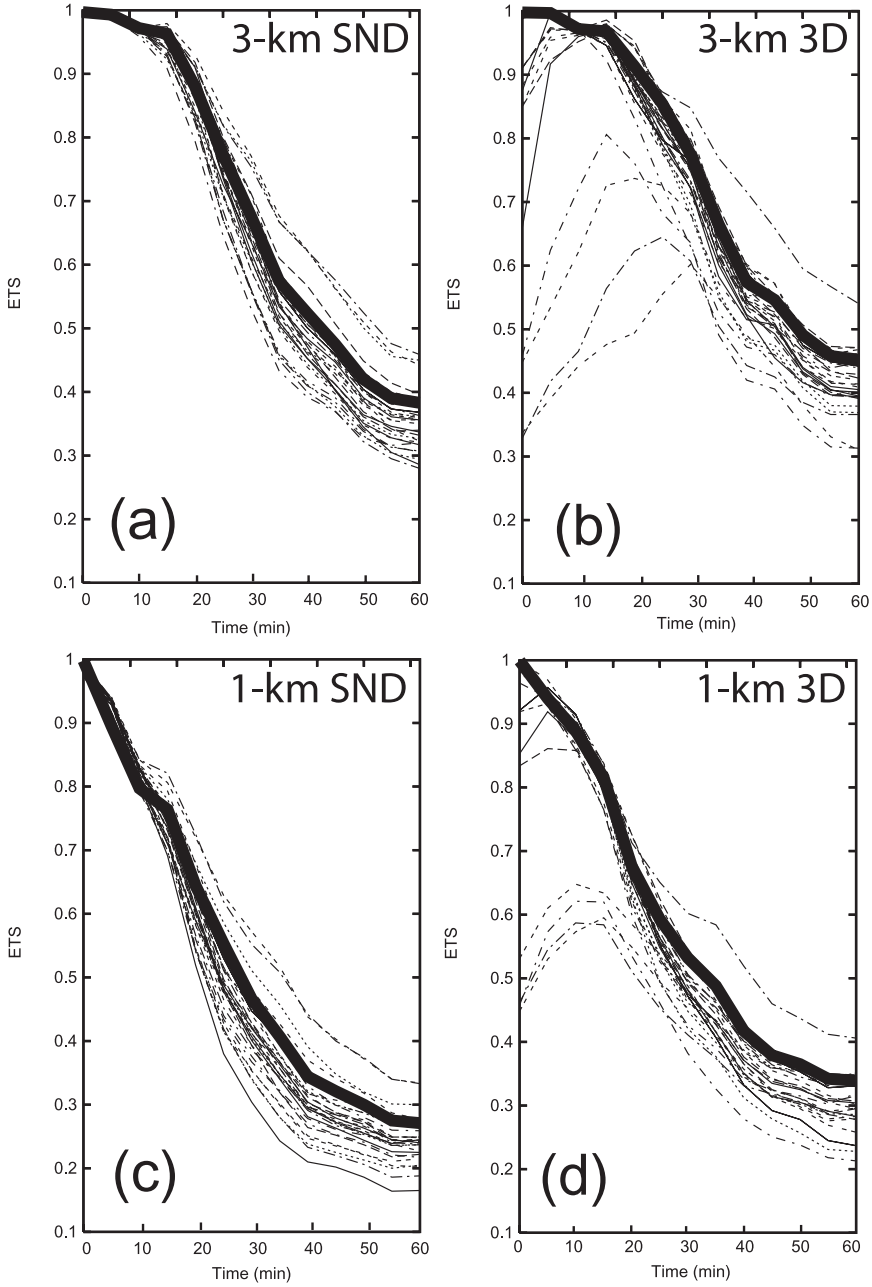

FIG. 16. Values of equitable threat score (ETS) for a 30-dBZ reflectivity threshold as a function of forecast time (min) from 30 ensemble members (thin lines) and the ensemble mean (thick line) for (a) 3-km SND, (b) 3-km 3D, (c) 1-km SND, and (d) 1-km 3D. The independent 3DVAR analyses of reflectivity are taken as truth.

Much more work is needed to understand how best to develop an ensemble forecasting system for severe convection in real-time settings. The importance of employing intermittent assimilation cycles within a 3DVAR deserves particular attention because cycling will help define the cold pools associated with the thunderstorms that can play an important role in thunderstorm evolution. The use of radar observations to suppress convection in regions where it is not observed, especially when convection exists in the model background fields, is particularly challenging. Our efforts in the future will include examining the role of grid nesting, cycling, evaluating other techniques for generating initial perturbations, and evaluating other data assimilation techniques, such as a storm-scale ensemble Kalman filter for convective ensemble forecasting.

Acknowledgments. This research was primarily funded by the National Severe Storm Laboratory under Grant NSSL/NOAA-085010. The second author was also supported by NSF Grants ATM-0738370, ATM-0802888, and EEC-031347. Dr. Fanyou Kong is acknowledged for providing us some statistical verification code. All of the numerical simulations were performed at the University of Oklahoma Supercomputer Center for Education and Research (OSCER). We appreciate Altug Aksoy and another anonymous reviewer for their very helpful suggestions.

REFERENCES

Adlerman, E. J., K. K. Droegemeier, and R. Davies-Jones, 1999: A numerical simulation of cyclic mesocyclogenesis. *J. Atmos. Sci.,* **56,** 2045–2069.

Aksoy, A., D. C. Dowell, and C. Snyder, 2009: A multicase comparative assessment of the ensemble Kalman filter for assimilation of radar observations. Part I: Storm-scale analyses. *Mon. Wea. Rev.,* **137,** 1805–1824.

Alberoni, P. P., and Coauthors, 2003: Quality and assimilation of radar data for NWP—A review. European Commission Rep. EUR 20600, COST 717 Review Rep., 38 pp.

Albers, S. C., J. A. McGinley, D. L. Birkenheuer, and J. R. Smart, 1996: The Local Analysis and Prediction System (LAPS): Analyses of clouds, precipitation, and temperature. *Wea. Forecasting,* **11,** 273–287.

Anderson, J. L., and N. Collins, 2007: Scalable implementations of ensemble filter algorithms for data assimilation. *J. Atmos. Oceanic Technol.,* **24,** 1452–1463.

Brewster, K., 2002: Recent advances in the diabatic initialization of a non-hydrostatic numerical model. Preprints, *15th Conf. on Numerical Weather Prediction/21st Conf. on Severe Local Storms,* San Antonio, TX, Amer. Meteor. Soc., J6.3. [Available online at http://ams.confex.com/ams/SLS_WAF_NWP/techprogram/paper_47414.htm.]

——, M. Hu, M. Xue, and J. Gao, 2005: Efficient assimilation of radar data at high resolution for short-range numerical weather prediction. *Extended Abstracts, World Weather Research Program Symp. on Nowcasting and Very Short-Range Forecasting,* Tolouse, France, World Meteorological Organization, 3.06.

Brooks, H. E., C. A. Doswell, and J. Cooper, 1994: On the environments of tornadic and nontornadic mesocyclones. *Wea. Forecasting,* **9,** 606–618.

——, M. S. Tracton, D. J. Stensrud, G. Dimego, and Z. Toth, 1995: Short-range ensemble forecasting: Report from a workshop (25–27 July 1994). *Bull. Amer. Meteor. Soc.,* **76,** 1617–1624.

Burgess, D. W., V. T. Wood, and R. A. Brown, 1982: Mesocyclone evolution statistics. Preprints, *12th Conf. on Severe Local Storms,* San Antonio, TX, Amer. Meteor. Soc., 422–424.

Crook, N. A., and J. Sun, 2004: Analysis and forecasting of the low-level wind during the Sydney 2000 Forecast Demonstration Project. *Wea. Forecasting,* **19,** 151–167.

Dowell, D. C., and H. B. Bluestein, 2002: The 8 June 1995 McLean, Texas, storm. Part I: Observations of cyclic tornadogenesis. *Mon. Wea. Rev.,* **130,** 2626–2648.

——, and L. J. Wicker, 2009: Additive noise for storm-scale ensemble data assimilation. *J. Atmos. Oceanic Technol.,* **26,** 911–927.

——, F. Zhang, L. J. Wicker, C. Snyder, and N. A. Crook, 2004: Wind and temperature retrievals in the 17 May 1981 Arcadia, Oklahoma, supercell: Ensemble Kalman filter experiments. *Mon. Wea. Rev.,* **132,** 1982–2005.

Du, J., and M. S. Tracton, 2001: Implementation of a real-time short-range ensemble forecasting system at NCEP: An update. Preprints, *Ninth Conf. on Mesoscale Processes,* Fort Lauderdale, FL, Amer. Meteor. Soc., P4.9. [Available online at http://ams.confex.com/ams/WAF-NWP-MESO/techprogram/paper_23074.htm.]

Elmore, K. L., D. J. Stensrud, and K. C. Crawford, 2002: Ensemble cloud model applications to forecasting thunderstorms. *J. Appl. Meteor.,* **41,** 363–383.

——, S. J. Weiss, and P. C. Banacos, 2003: Operational ensemble cloud model forecasts: Some preliminary results. *Wea. Forecasting,* **18,** 953–964.

Evensen, G., 1997: Advanced data assimilation for strongly nonlinear dynamics. *Mon. Wea. Rev.,* **125,** 1342–1354.

Fujita, T., D. J. Stensrud, and D. C. Dowell, 2007: Surface data assimilation using an ensemble Kalman filter approach with initial condition and model physics uncertainty. *Mon. Wea. Rev.,* **135,** 1846–1868.

——, ——, and ——, 2008: Using precipitation observations in a mesoscale short-range ensemble analysis and forecasting system. *Wea. Forecasting,* **23,** 357–372.

Gallus, W. A., 2002: Impact of verification grid-box size on warm-season QPF skill measures. *Wea. Forecasting,* **17,** 1296–1302.

Gao, J., M. Xue, K. Brewster, F. Carr, and K. K. Droegemeier, 2002: New development of a 3DVAR system for a nonhydrostatic NWP model. Preprints, *15th Conf. on Numerical Weather Prediction/19th Conf. on Weather Analysis and Forecasting,* San Antonio, TX, Amer. Meteor. Soc., P12.4. [Available online at http://ams.confex.com/ams/pdfpapers/47480.pdf.]

——, ——, ——, and ——, 2003: A 3DVAR method for Doppler radar wind assimilation with recursive filter. Preprints, *31st Int. Conf. on Radar Meteorology,* Seattle, WA, Amer. Meteor. Soc., P1C.4. [Available online at http://ams.confex.com/ams/32BC31R5C/techprogram/paper_64579.htm.]

——, ——, ——, and ——, 2004: A three-dimensional variational data assimilation method with recursive filter for single-Doppler radar. *J. Atmos. Oceanic Technol.,* **21,** 457–469.

Hamill, T. M., S. L. Mullen, C. Snyder, and Z. Toth, 2000: Ensemble forecasting in the short to medium range: Report from a workshop. *Bull. Amer. Meteor. Soc.,* **81,** 2653–2664.

Hou, D., E. Kalnay, and K. K. Droegemeier, 2001: Objective verification of the SAMEX'98 ensemble forecasts. *Mon. Wea. Rev.,* **129,** 73–91.

Hu, M., and M. Xue, 2002: Sensitivity of model thunderstorms to modifications to the environmental conditions by a nearby thunderstorm in the prediction of 2000 Fort Worth tornado case. Preprints, *15th Conf. on Numerical Weather Prediction/19th Conf. on Weather Analysis and Forecasting,* San Antonio, TX, Amer. Meteor. Soc., P2.1. [Available online at http://ams.confex.com/ams/pdfpapers/47580.pdf.]

——, and ——, 2007: Impact of configurations of rapid intermittent assimilation of WSR-88D radar data for the 8 May 2003 Oklahoma City tornadic thunderstorm case. *Mon. Wea. Rev.,* **135,** 507–525.

——, ——, and K. Brewster, 2006a: 3DVAR and cloud analysis with WSR-88D level-II data for the prediction of Fort Worth tornadic thunderstorms. Part I: Cloud analysis and its impact. *Mon. Wea. Rev.,* **134,** 675–698.

——, ——, J. Gao, and K. Brewster, 2006b: 3DVAR and cloud analysis with WSR-88D level-II data for the prediction of the Fort Worth, Texas, tornadic thunderstorms. Part II: Impact

of radial velocity analysis via 3DVAR. *Mon. Wea. Rev.,* **134,** 699–721.

Johns, R. H., and J. A. Hart, 1993: Differentiating between types of severe thunderstorm outbreaks: A preliminary investigation. Preprints, *17th Conf. on Severe Local Storms,* St. Louis, MO, Amer. Meteor. Soc., 46–50.

Klemp, J., 2004: Next-generation mesoscale modeling: A technical overview of WRF. Preprints, *20th Conf. on Weather Analysis and Forecasting,* Seattle, WA, Amer. Meteor. Soc., P11.2.

Kong, F., K. K. Droegemeier, and N. L. Hickmon, 2006: Multiresolution ensemble forecasts of an observed tornadic thunderstorm system. Part I: Comparison of coarse- and fine-grid experiments. *Mon. Wea. Rev.,* **134,** 807–833.

——, ——, and ——, 2007: Multiresolution ensemble forecasts of an observed tornadic thunderstorm system. Part II: Storm-scale experiments. *Mon. Wea. Rev.,* **135,** 759–782.

Krishnamurti, T. N., and Coauthors, 2001: Real-time multianalysis–multimodel superensemble forecasts of precipitation using TRMM and SSM/I products. *Mon. Wea. Rev.,* **129,** 2861–2883.

Lemon, L. R., and M. Umscheid, 2008: The Greensburg, Kansas, tornadic storm: A storm of extremes. Preprints, *24th Conf. on Severe Local Storms,* Savannah, GA, Amer. Meteor. Soc., P2.4. [Available online at http://ams.confex.com/ams/pdfpapers/141811.pdf.]

Lewis, J., 2005: Roots of ensemble forecasting. *Mon. Wea. Rev.,* **133,** 1865–1885.

Lin, Y., P. S. Ray, and K. W. Johnson, 1993: Initialization of a modeled convective storm using Doppler radar–derived fields. *Mon. Wea. Rev.,* **121,** 2757–2775.

McCarthy, D., L. Ruthi, and J. Hutton, 2007: The Greensburg, KS, tornado. Preprints, *22nd Conf. on Weather Analysis and Forecasting/18th Conf. on Numerical Weather Prediction,* Park City, UT, Amer. Meteor. Soc., PJ2.4.

Montmerle, T., and C. Faccani, 2009: Mesoscale assimilation of radial velocities from Doppler radars in a preoperational framework. *Mon. Wea. Rev.,* **137,** 1939–1953.

Purser, R. J., W.-S. Wu, D. Parrish, and N. M. Roberts, 2003a: Numerical aspects of the application of recursive filters to variational statistical analysis. Part I: Spatially homogeneous and isotropic Gaussian covariances. *Mon. Wea. Rev.,* **131,** 1524–1535.

——, ——, ——, and ——, 2003b: Numerical aspects of the application of recursive filters to variational statistical analysis. Part II: Spatially inhomogeneous and anisotropic general covariances. *Mon. Wea. Rev.,* **131,** 1536–1548.

Rasmussen, E. N., and D. O. Blanchard, 1998: A baseline climatology of sounding-derived supercell and tornado forecast parameters. *Wea. Forecasting,* **13,** 1148–1164.

Rotunno, R., and J. B. Klemp, 1982: The influence of the shear-induced pressure gradient on thunderstorm motion. *Mon. Wea. Rev.,* **110,** 136–151.

——, and ——, 1985: On the rotation and propagation of simulated supercell thunderstorms. *J. Atmos. Sci.,* **42,** 271–292.

Snyder, C., and F. Zhang, 2003: Assimilation of simulated Doppler radar observations with an ensemble Kalman filter. *Mon. Wea. Rev.,* **131,** 1663–1677.

Stensrud, D. J., and S. J. Weiss, 2002: Mesoscale model ensemble forecasts of the 3 May 1999 tornado outbreak. *Wea. Forecasting,* **17,** 526–543.

——, and N. Yussouf, 2007: Reliable probabilistic quantitative precipitation forecasts from a short-range ensemble forecasting system. *Wea. Forecasting,* **22,** 3–17.

——, J.-W. Bao, and T. T. Warner, 2000: Using initial condition and model physics perturbations in short-range ensembles. *Mon. Wea. Rev.,* **128,** 2077–2107.

——, N. Yussouf, D. C. Dowell, and M. C. Coniglio, 2009: Assimilating surface data into a mesoscale model ensemble: Cold pool analyses from spring 2007. *Atmos. Res.,* **93,** 207–220.

Sun, J., and N. A. Crook, 1998: Dynamical and microphysical retrieval from Doppler radar observations using a cloud model and its adjoint. Part II: Retrieval experiments of an observed Florida convective storm. *J. Atmos. Sci.,* **55,** 835–852.

Thompson, R. L., and R. Edwards, 2000: An overview of environmental conditions and forecast implications of the 3 May 1999 tornado outbreak. *Wea. Forecasting,* **15,** 682–699.

——, ——, J. A. Hart, K. L. Elmore, and P. Markowski, 2003: Close proximity soundings within supercell environments obtained from the Rapid Update Cycle. *Wea. Forecasting,* **18,** 1243–1261.

Tong, M., and M. Xue, 2005: Ensemble Kalman filter assimilation of Doppler radar data with a compressible nonhydrostatic model: OSS experiments. *Mon. Wea. Rev.,* **133,** 1789–1807.

Torn, R. D., G. J. Hakim, and C. Snyder, 2006: Boundary conditions for limited-area ensemble Kalman filters. *Mon. Wea. Rev.,* **134,** 2490–2502.

Weisman, M. L., and J. B. Klemp, 1984: The structure and classification of numerically simulated convective storms in directionally varying wind shears. *Mon. Wea. Rev.,* **112,** 2479–2498.

Wilks, D. S., 2006: *Statistical Methods in the Atmospheric Sciences*. 2nd ed. Academic Press, 627 pp.

Xiao, Q., Y.-H. Kuo, J. Sun, W.-C. Lee, E. Lim, Y.-R. Guo, and D. M. Barker, 2005: Assimilation of Doppler radar velocities with a regional 3DVAR system: Impact of Doppler velocities on forecasts of a heavy rainfall case. *J. Appl. Meteor.,* **44,** 768–788.

Xue, M., K. K. Droegemeier, and V. Wong, 2000: The Advanced Regional Prediction System (ARPS)—A multiscale nonhydrostatic atmospheric simulation and prediction model. Part I: Model dynamics and verification. *Meteor. Atmos. Phys.,* **75,** 161–193.

——, and Coauthors, 2001: The Advanced Regional Prediction System (ARPS)—A multiscale nonhydrostatic atmospheric simulation and prediction tool. Part II: Model physics and applications. *Meteor. Atmos. Phys.,* **76,** 134–165.

——, D. Wang, J. Gao, K. Brewster, and K. K. Droegemeier, 2003: The Advanced Regional Prediction System (ARPS), storm-scale numerical weather prediction and data assimilation. *Meteor. Atmos. Phys.,* **82,** 143–165.

——, and Coauthors, 2008: CAPS real-time storm-scale ensemble and high-resolution forecasts as part of the NOAA Hazardous Weather Test bed 2008 spring experiment. Preprints, *24th Conf. on Severe Local Storms,* Savannah, GA, Amer. Meteor. Soc., P12.2. [Available online at http://twister.ou.edu/papers/Xue_24SLS_conf_2008SpringExperiment.pdf.]

Yussouf, N., and D. J. Stensrud, 2006: Prediction of near-surface variables at independent locations from a bias-corrected ensemble forecasting system. *Mon. Wea. Rev.,* **134,** 3415–3424.

Zhang, J., F. Carr, and K. Brewster, 1998: ADAS cloud analysis. Preprints, *12th Conf. on Numerical Weather Prediction,* Phoenix, AZ, Amer. Meteor. Soc., 185–188.

Zhao, K., and M. Xue, 2009: Assimilation of coastal Doppler radar data with the ARPS 3DVAR and cloud analysis for the prediction of Hurricane Ike (2008). *Geophys. Res. Lett.,* **36,** L12803, doi:10.1029/2009GL038658.